

Microlasers Enabled by Soft-Matter Technology

Van Duong Ta, Yue Wang, and Handong Sun*

Soft-matter microlasers are an interesting part of soft-matter photonics, which are based on liquids, liquid crystals, polymers, biological materials, and fabricated mainly by solution-processing approaches. Soft-matter microlasers comprehend a multitude of attractive features, including low-cost, mechanical flexibility, wide range wavelength tunability and, in some cases, biocompatibility, and biodegradability. As such, they are recognized as versatile candidates for efficient light sources with enhanced performances and applications as ultrasensitive physical, chemical, and biological sensors. Here, the recent developments of soft-matter microlasers are reviewed in time and the prospect in this field is provided. First, the characteristics of the representative soft-matter microlasers are discussed with focus on their laser structures, lasing mechanisms, fabrication approaches, and gain material origins, followed by an introduction about the current cutting-edge soft-technologies that are applied in soft-matter microlasers. Afterward, their potential applications as wavelength tunable sources, sensors, and displays are highlighted. Finally, the work is summarized and the prospect of soft-matter microlasers for expanding this emerging research field is presented.

instance, the motivation of more efficient light sources has driven research interests in control of the spontaneous emission via Purcell effect^[2] and the strong coupling regime (between exciton and photon) in order to realize a nonthreshold polariton laser.^[3,4] With regard to practical uses, microlasers are vital components in photonic integrated circuits (PICs), on-chip communication, bioimaging, and label-free sensing.^[5]

A microlaser consists of three main elements: an optical microcavity, an active medium, and a pumping source. The active material provides radiative emission upon being pumped either optically or electrically, which is then trapped and modulated by resonant recirculation via the microcavity. When the optical gain in the microcavity reaches the total optical losses, the system surpasses a threshold and it starts to lase.^[6] Similar to conventional lasers (except that microlasers have a much smaller size), microlasers generally

provide coherent, monochromatic, and, in many cases, collimated light beam. The motivation of research on microlasers is producing high quality, low-cost laser sources with controllable size (may be down to nanoscale), configuration, and employing them for practical applications in photonic devices, optical sensors, and bioimaging.^[5]

Generally, as shown in **Figure 1**, microcavities can be classified into different types accordingly to the confinement mechanism for light amplification.^[1] Typical configurations are Fabry–Pérot (FP) cavities (Figure 1a), distributed feedback (DFB) cavities (Figure 1b), whispering gallery mode (WGM) cavities (Figure 1c), and photonic crystal cavities (not shown here, as it is less popular for soft-matter lasers). FP cavities provide optical feedback based on two highly reflective parallel mirrors. In many cases, 1D structure like wires or rods may act as fine FP optical cavities because their two end facets work as efficient reflectors. The first laser made by Maiman in 1960 is a good example of a FP laser.^[7] DFB cavities rely on a diffractive grating, which is designed to effectively reflect only a specific wavelength (generally around the maximum emission of active medium). Consequently, single-mode emission is frequently observed from DFB lasers. WGM cavities confine light by the effective multiple total internal reflections at the interface between the cavity and its surrounding medium. Common WGM cavity geometries are microspheres, microdisks, microfibers, and microcapillaries. WGM cavities usually exhibit high quality (Q) factors and small mode volumes, a requirement for low-threshold lasers.^[1]

1. Introduction


Microlasers are tiny lasers whose sizes are close to the dimension of the emission wavelength. Due to their footprint miniaturization, microlasers have been demonstrated as attractive platforms for both fundamental studies of light–matter interaction and a wide range of practical applications.^[1] For

Dr. V. D. Ta
Department of Optical Devices
Le Quy Don Technical University
236 Hoang Quoc Viet, Hanoi 100000, Vietnam

Dr. Y. Wang, Prof. H. D. Sun
Division of Physics and Applied Physics
School of Physical and Mathematical Sciences
Nanyang Technological University
Singapore 637371, Singapore
E-mail: hdsun@ntu.edu.sg

Prof. H. D. Sun
Centre for Disruptive Photonic Technologies (CDPT)
Nanyang Technological University
Singapore 637371, Singapore

Prof. H. D. Sun
MajuLab
CNRS-UCA-SU-NUS-NTU International Joint Research Unit
Singapore 637371, Singapore

 The ORCID identification number(s) for the author(s) of this article can be found under <https://doi.org/10.1002/adom.201900057>.

DOI: 10.1002/adom.201900057

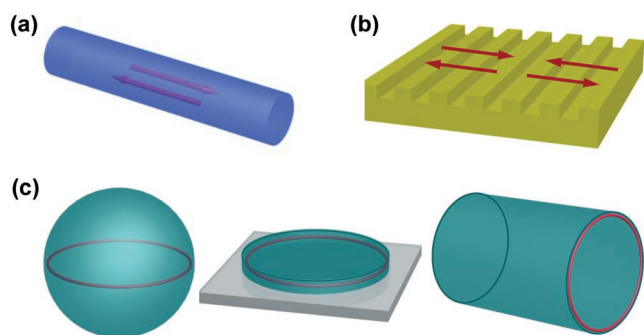


Figure 1. Typical microcavity configurations according to the confinement method used for light amplification in soft-matter microlasers. a) Fabry–Perot microcavity. b) Distributed feedback microcavity. c) Whispering gallery mode microcavities. From left to right, microsphere, microdisk, microfiber, or microcapillary. The red arrows and circle lines indicate the main propagation direction of photons in the microcavities.

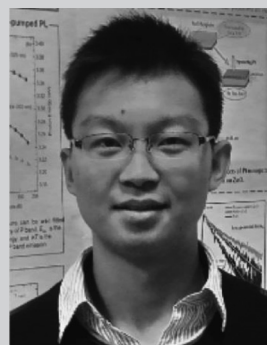
In 1989, the first vertical-cavity surface emitting microlasers based on single-quantum well (GaInAs) were fabricated.^[8] This innovation has triggered more research attention on microlasers. Pioneering works mainly relied on conventional semiconductors using a variety of structures such as microdisks,^[9] microspheres,^[10,11] photonic crystals,^[12] and nanowires.^[13] However, the conventional semiconductor lasers have drawbacks including complex nano/microfabrication, high-cost, and mechanical rigidity.

Further research on novel materials would provide additional flexibility to current fabrication methods of microlasers and enhance their performances. For example, recently developed materials such as nanocrystal quantum dots (NQDs),^[14–16] perovskite materials,^[17–21] organic semiconductors^[22] would provide additional capability for the bottom-up fabrication of current microlasers. Among these available supplies, organic materials are a fascinating and flexible candidate for optics and photonics owing to their high transparency, cost-effectiveness, mechanical flexibility, and lightweight.^[23] For applications in laser devices, organic materials can serve as an active medium and a cavity matrix. For the first case, various gain materials including organic dyes, NQDs can be doped into organic cavities to produce laser devices with high levels of mechanical and color tunability.^[24]

In the literature, there have been several review articles on organic lasers with the main focus on conducting polymers.^[25–30] Furthermore, organic lasers also are partly covered in a number of review papers dedicated to specific laser structures such as optofluidic lasers,^[31–33] droplet lasers,^[34–36] whispering gallery mode lasers.^[37–41] However, none of them is specifically devoted to soft-matter lasers. Actually, the materials used in organic lasers can be liquids (for instance, organic oil and solvents), liquid crystals, polymers, and a numerous biological feature, all of which are included in one class of matter, soft-matter. They share similar physical properties like easy to deform by mechanical stress and thermal fluctuations. Recently, soft-matter based lasers are emerging as an attractive candidate for a variety of optical and photonic applications including electrically tunable lasers,^[42] lightweight and flexible plastic lasers,^[43] high-resolution laser-based displays,^[44]



Van Duong Ta is currently a lecturer at Department of Optical Devices, Le Quy Don Technical University, Vietnam. He received his Diploma in Optoelectronics and Laser Systems from Bauman Moscow State Technical University, Russia, and received a PhD in physics from Nanyang Technological University, Singapore. His main research interests are whispering gallery mode microlasers, biolasers, micrometer-sized random lasers, and their biosensing applications.



Yue Wang received his bachelor's degree in materials science from Sichuan University, China, and his PhD degree in physics from Nanyang Technological University, Singapore. He is currently carrying out his postdoctoral work with Prof. Handong Sun at Nanyang Technological University. His research interests include optical spectroscopy, semiconductor photophysics, and optically pumped lasers.



Handong Sun is currently working as an associate professor in the School of Physical and Mathematical Sciences at Nanyang Technological University, Singapore. He received his bachelor's degree in physics from Dalian University of Technology, Master's and PhD degrees from Huazhong University of Science and Technology, China, and Hong Kong University of Science and Technology, respectively. He is a fellow of the American Physical Society. His research interests are focused on light–matter interactions, including the spectroscopic characterization of inorganic, organic, and hybrid materials, as well as the underlying physics behind optoelectronic devices.

intracellular biosensing, and cell tracking.^[45,46] As a result, a review of this emerging topic is necessary for a complete vision of a widespread research area. In this report, we will provide the progress of soft-matter lasers over various aspects. First, we focus on droplet lasers—a typical kind of soft-matter lasers,

followed by stressing the recent achievements of polymer lasers, biomaterial lasers, the typical and novel materials used for lasers. After that, we examine the soft-technology applied for fabrication of microlasers, followed by the applications of soft-matter microlasers. Finally, a summary and our personal view on the prospects of soft-matter microlasers are given.

2. Soft-Matter Microlasers: Soft Materials

2.1. Soft-Matter Microlasers Developed from Liquid Droplets

The idea of using a spherical structure for light amplification was proposed soon after the first laser was made. In 1961, Garrett et al. at Bell Laboratories observed for the first time lasing emission from an ≈ 1 mm diameter spherical sample of $\text{CaF}_2:\text{Sm}^{++}$.^[47] The result confirms that a sphere is a versatile geometry for laser generation. Garrett et al. realized that the light was confined inside the sphere by effective multiple total internal reflections at the sphere–air interface. The trapped light travelled roughly circumferentially (many round trips) inside the surface of the sphere, leading to light amplification. This observation is similar to the analogous phenomenon in acoustics that was observed and reported by Rayleigh in the early 20th century.^[48] As a result, Garrett et al. used the term “whispering modes” to describe the sphere laser. Further miniaturization of lasers was not an easy task at that age. It took nearly 20 years until Chang’s group reported the observation of WGM resonances in dye-impregnated single polystyrene (PS) microspheres.^[49] In this work, the cavity size was significantly reduced compared to the previous work of Garrett et al. The microsphere was only ≈ 10 μm in diameter (two orders of magnitude smaller). Even though lasing emission was not observed, it was a milestone toward microlasers.

On the basis of the above work, it has been expected that a liquid droplet can also act as a suitable cavity for lasers. It would be interesting to see lasing emission from a structure as fragile as a droplet.^[36] However, due to the inherent property of any fluid, a droplet generally cannot be formed on a conventional substrate without spreading. As a result, it is required to establish a suitable technique to generate measurable droplets in order to produce droplet lasers. In 1984, Chang’s group finally made a breakthrough after a long time investigation.^[50] They reported for the first time droplet lasers based on dye-doped ethanol microdroplets. Following this work, additional lasing characteristics and applications of droplet lasers were subsequently studied.^[51,52]

2.1.1. Free-Falling and Free-Standing Droplet Lasers

Figure 2a shows the approach that Chang’s group used to obtain droplet lasers.^[52] First, organic dye molecules (Rhodamine 590 or Rhodamine 640) were doped to ethanol. Then, the solution was injected to a modified piezoelectric vibrating-orifice aerosol generator. When applying electric power to the system, a stream of droplets was continuously formed. The droplet diameter can be varied from 20 to 40 μm , depending on the frequency of the oscillator. A pulsed laser was used to

irradiate the droplets and their fluorescence image was captured by a camera. As shown in **Figure 2b**, the incident green laser is visible in form of two spots at front and back interfaces. When a filter blocks the pumping laser, red emission is clearly seen throughout the droplet–air interface (**Figure 2c**). It is because the emission from the dye molecules is coupled into WGM that circumnavigates in a circular loop near the surface of the droplet. This observation supports WGMs as an optical feedback mechanism for light amplification. When using a crossed polarization analyzer, the red and the green emissions are deleted simultaneously (**Figure 2d**).

In general, the lasing wavelengths come from a WGM laser and can be well fitted by explicit asymptotic formulas^[53]

$$(\lambda_m^q)^{-1} = \frac{1}{\pi D n_1} \left[\nu + 2^{-1/3} A_q \nu^{1/3} - \frac{P}{\sqrt{n_r^2 - 1}} + \frac{2^{-2/3} A_q^2 \nu^{-1/3}}{10/3} - \frac{P \left(n_r^2 - \frac{2}{3} P^2 \right) A_q}{2^{1/3} (n_r^2 - 1)^{3/2} \nu^{2/3}} \right] \quad (1)$$

where D is the diameter of the circular microcavity; $\nu = m + 0.5$, m is the azimuthal mode number; $n_r = n_1/n_2$ with n_1 and n_2 are refractive indexes of the cavity and outside medium, respectively; A_q is the root of the Airy function, where q is the radial mode number; $A_q = 2.338, 4.088, 5.521$ for $q = 1, 2, 3$, respectively. P is a coefficient related to the polarization characteristic and is given $P = 1/n_r$ for transverse magnetic (TM) modes, and $P = n_r$ for transverse electric (TE) modes. In principle, the first radial mode number ($q = 1$) has the highest Q factor so the lasing wavelengths of this fundamental mode are the most observable in comparison with higher modes ($q > 1$). For $q = 1$, the lasing wavelength can be estimated as^[54]

$$\lambda = \frac{\pi D n_{\text{eff}}}{m} \quad (2)$$

where, n_{eff} is the effective refractive index of the cavity.

From Equation (2), it is easy to derive the free spectral range (FSR) or mode spacing of the lasing modes, which is defined as the distance between successive azimuthal mode number

$$\text{FSR} = \frac{\lambda^2}{\pi n_{\text{eff}} D} \quad (3)$$

The above WGM theory can well explain the lasing spectrum obtained by Chang’s group. The lasing emission highlights liquid–air boundary, enabling accurate determination of droplet size. Another way to determine the droplet size is by using Equation (3), as the mode spacing is easily measured from the emission spectrum. As a result, laser photograph and laser emission would be a novel approach for studying droplet dynamics such as size, shape, and orientation.

The free-falling droplets developed by Chang’s group are suitable for the study of droplet dynamics. Nonetheless, due to the nonuniformity in droplet size, this technique is not ideal for the study of laser characteristics. Instead, optical levitation of single liquid drops is more appropriate for this purpose.^[55] **Figure 2e** illustrates a similar approach using electrodynamic levitation system for generating a free-standing drop.^[56] In this work, the droplet was composed of $\approx 70\%$ water, $\approx 30\%$ glycerine

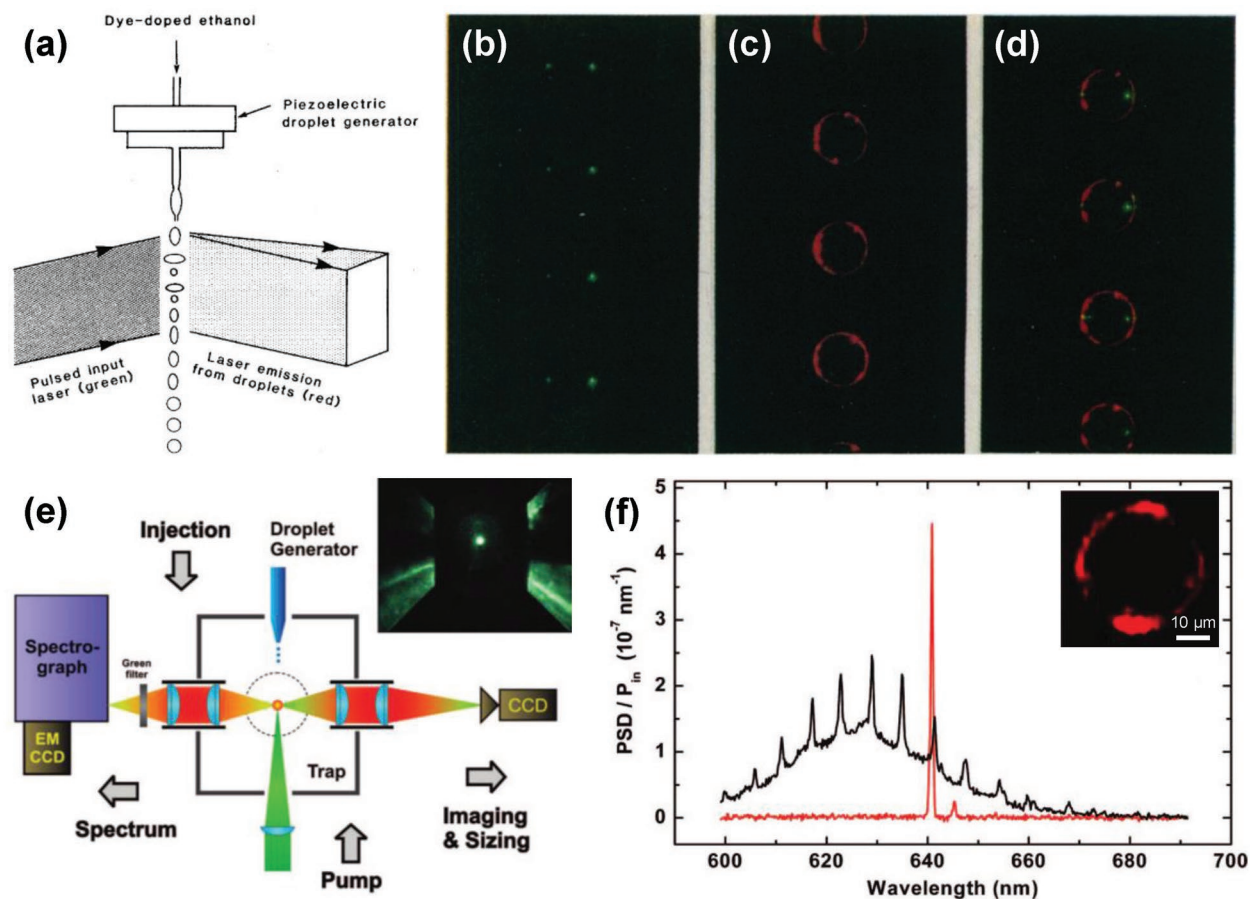


Figure 2. a) Schematic diagram of the experimental setup for the realization of laser emission from free-falling droplets. b–d) Optical fluorescence images of a stream of droplets irradiated by a pulsed green (532 nm) laser. Reproduced with permission.^[52] Copyright 1986, The American Association for the Advancement of Science. e) Schematic diagram of the optical apparatus for generating and levitating a microdrop laser. f) Fluorescence and lasing spectra of a 9 μm droplet with CdSe/ZnS NQDs. Single mode lasing (red curve) compared with WGM resonance (black curve). Power spectral density (PSD) is normalized to the cross-sectional pump power. The inset shows a fluorescence image of a 40 μm droplet exhibits a red ring feature like free-falling droplets in (c). Reproduced with permission.^[56] Copyright 2008, American Chemical Society.

(in order to reduce evaporation), and water-soluble CdSe/ZnS core-shell NQDs. First, droplets are injected from the top through a microdrop generator. Next, they are charged by fluid jet polarization technique. An AC electric field is applied to the trapping system to balance the gravity and fix droplet's position. The size of the droplets can be varied from 10 to 50 μm. The trapped droplet is irradiated from the bottom by a pulse laser. Figure 2f plots emission from a 9 μm droplet below and above the lasing threshold of 53 mJ cm⁻². Below the threshold, WGM is observed on top of the fluorescence spectrum (black curve). Above the threshold, single lasing mode is observed on a flat background due to the suppression of the fluorescence. It is worth noting that multimode lasing is common for WGM lasers. Herein, single mode emission is obtained primarily due to two reasons: i) the small droplet size (9 μm in diameter) and ii) the narrow spectral gain profile. From spectral measurements, the *Q* factor of lasing modes is about 6.5 × 10³. Owing to the high *Q* value and solution-based processing, this system provides a versatile method for future studies of the lasing properties of different gain media.

2.1.2. Droplet Lasers on Superhydrophobic Surfaces

The trapping technique in the prior work seems to be a feasible tool for forming a free-standing droplet. However, it is still a complex system. It requires an AC field and well-training skills for operation. An alternative solution, which is supposed to be simpler, to obtain stationary droplets is using superhydrophobic or ultrahydrophobic surfaces.^[57] Droplets on these nonwettable surfaces have almost perfectly spherical shape with very high water contact angles, generally >150°. Superhydrophobic surfaces are commonly obtained by either coating hydrophobic materials or creating rough structures on conventional surfaces.^[58,59] In 2007, Kiraz's group reported droplet lasers located on a superhydrophobic surface that was fabricated by spin coating hydrophobic silica nanoparticles on a glass substrate.^[60] To generate small droplets, an ultrasonic nebulizer was used to spray Rhodamine B (RhB) doped water/glycerol solution onto the coated surface. The final droplets have sizes which range from a few μm to 20 μm. Based on the same technique, Kiraz's group and other scientists have demonstrated a

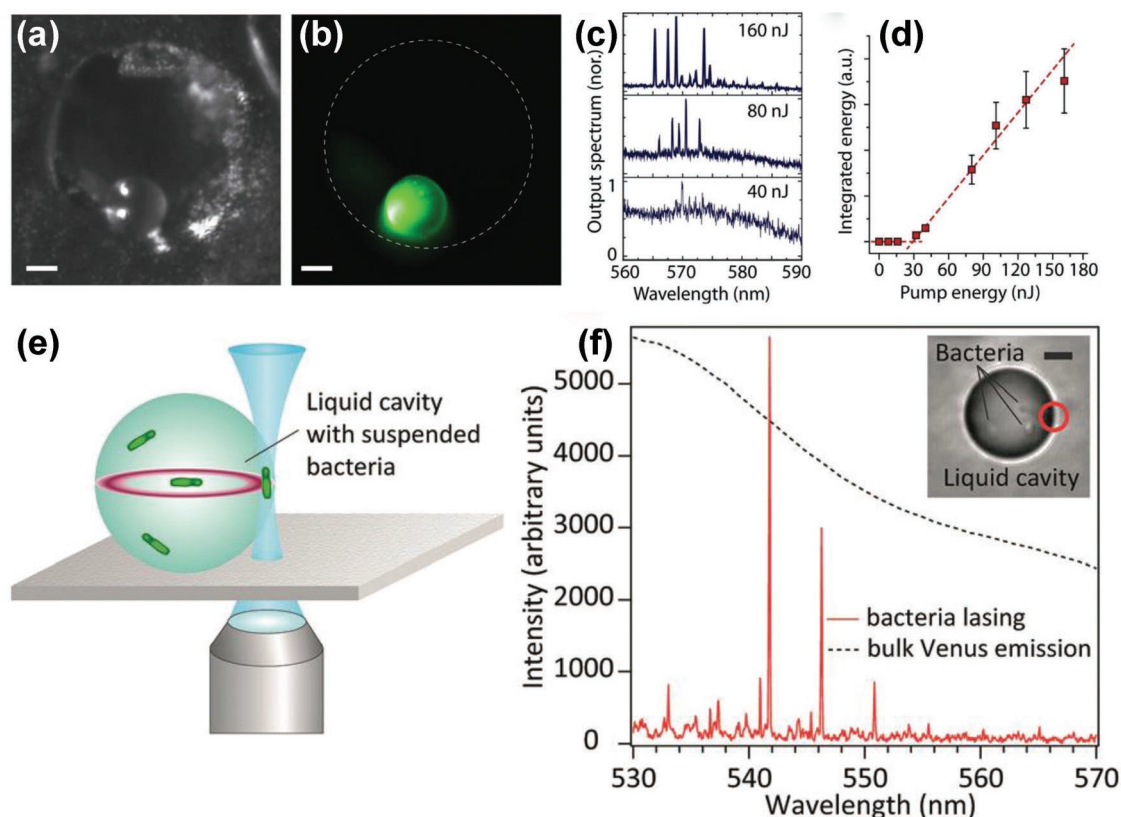


Figure 3. a) An optical image of a vitamin microdroplet in a super-hydrophobic poly-L-lactic acid well and b) its corresponding fluorescence image above the lasing threshold. c) Normalized laser emission spectra under various pump pulse energies. d) Integrated energy of the laser peaks versus pump energy. Scale bars are 10 μm . Reproduced with permission.^[64] Copyright 2013, Wiley-VCH. e) Experimental setup for observation of a laser drop that contains live *E. coli* bacterial cells expressing Venus fluorescent protein. f) A typical lasing emission spectrum (solid line) obtained from a droplet (shown in the inset) with suspended *E. coli* bacterial cells. The droplet was irradiated at the edge indicated by a circle. The scale bar is 5 μm . Reproduced with permission.^[66] Copyright 2014, Royal Society of Chemistry.

number of interesting phenomena such as Raman lasing,^[61,62] and spectral tuning from stationary microdroplets.^[63]

It has been demonstrated that superhydrophobic surfaces are an adaptable method for investigation of novel water-soluble gain media. Recently, this method has been employed for studying biomaterials as new lasing media. **Figure 3a,b** shows micrographs of a single flavin mononucleotide (FMN) microdrop formed in a hydrophobic microwell.^[64] The droplet was also generated by spraying the FMN solution. The droplet did not spread because the well was coated with a synthetic hydrophobic biopolymer, polylactic acid. Specifically, this biocompatible material is approved for human clinical and ecological uses.^[65] To investigate lasing properties, the droplet was pumped by a focus laser beam at the wavelength of 460 nm. The emission spectra of the droplet are plotted in **Figure 3c**. The lasing intensity and the number of lasing modes increased with increasing pulse energy. The lasing threshold was determined to be very low, only about 30 nJ (**Figure 3d**). The spectral linewidth of the mode was 0.19 nm, corresponding to a Q factor of 3×10^3 . Remarkably, the microdroplets exhibited excellent properties, retaining their lasing output after storage at ambient condition for several days. Owing to the biocompatibility, these lasers are potential for in vivo biosensing (will be discussed in Section 4).

Fluorescent biological molecules have been reported as sources of lasing emission as shown in **Figure 3e,f**.^[66] Droplets were generated by spraying a mixture of water and glycerol with fluorescent bacteria over the surface. The droplets contained ≈ 5 –15 bacteria per droplet with a radius of ≈ 5 –10 μm . The droplets were excited by a focused laser beam at the droplet rim and at the position where contained the bacteria (**Figure 3e**). A typical emission spectrum from a 16.8 μm diameter droplet contains ≈ 7 bacterial cells at a pumping fluence of 312 mJ cm^{-2} (**Figure 3f**). High intensity and sharp lasing modes observed compared with broad emission of bulk Venus (expressed from the bacteria) solution. The spectral linewidth of lasing WGMs is 0.13 nm, which is comparable to other works on droplet lasers. This work shows that fluorescent *E. coli* bacteria expressing Venus is feasible as a gain medium for biolasers and promising for live-cell biosensors.

2.1.3. Floating Droplet Lasers

We have seen that droplets in various forms including free-falling droplets, free-standing (levitated) droplets, and stationary droplets (located on superhydrophobic surfaces) support laser generation. For these droplets, even though the

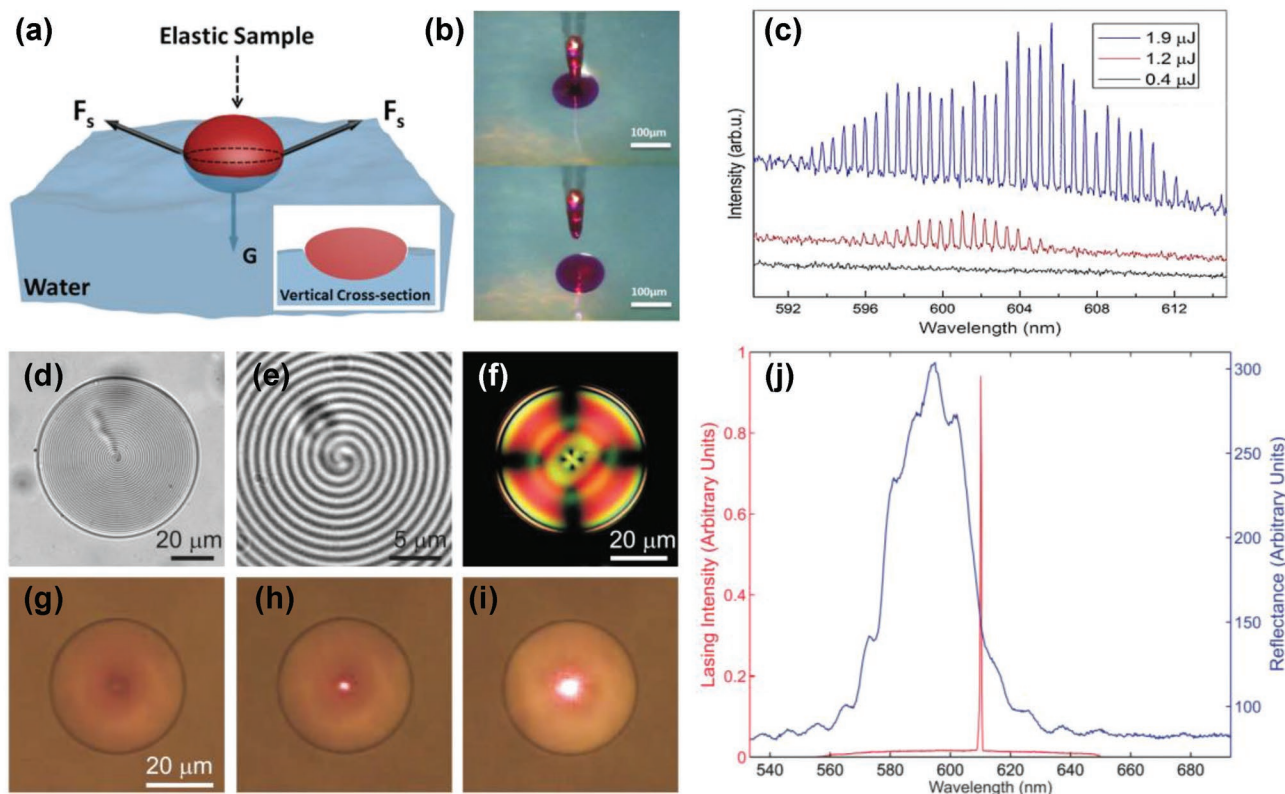


Figure 4. a) Illustration of a floating microlaser. Due to the variation of surface tension at the interfaces of droplet/water and droplet/air, the droplet has an asymmetric ellipsoid shape as shown in the inset. b) Droplet formation on water surface using a glass microtip. c) Emission spectra from a typical droplet under three different pumping energies. Reproduced under the terms of a Creative Commons Attribution 4.0 License.^[67] Copyright 2016, The Authors. d) A microscope image of a typical cholesteric droplet in glycerol. The concentric shells exhibit the light and dark color which is due to the variation of the refractive index of the droplet in the radial direction. e) High magnification of the center of the cholesteric droplet. f) A cholesteric droplet with PBC in the visible range of light, viewed under crossed polarizers and white light illumination. g–i) Droplets under pulsed laser irradiation ($\lambda = 532$ nm) when below the lasing threshold, at the threshold and above the threshold, respectively. j) Normalized lasing spectrum of a single CLC droplet and the reflection of a $30 \mu\text{m}$ planar cell filled with the same CLC mixture. Reproduced with permission.^[75] Copyright 2010, Optical Society of America.

laser cavity is flexible (due to the intrinsic property of liquid), the tunability of droplet size is highly limited. The change of droplet size is generally accomplished by evaporation. To obtain reconfigurable liquid droplet resonators is still a challenging issue. To overcome this drawback, Sun's group proposed a new type of liquid droplets that float on the water surface, as shown in **Figure 4a**.^[67] The droplet was composed of the epoxy resin (Araldite 506, Sigma-Aldrich) and Rhodamine 6G (R6G). Droplets were simultaneously formed by dispensing the doped compound onto the soap water surface (Figure 4b). The final geometry of droplets (either disk or ellipsoid) is related to the surface tension of water that can be well-controlled by a surfactant (simply a soap solution in this case). Figure 4c plots lasing spectra of a typical droplet with a size of $135 \mu\text{m}$ in diameter. By adding different quantities of surfactant, the droplet cavity will change correspondingly. It has been demonstrated that a droplet cavity can be bidirectionally and reversibly tuned (either become larger or smaller) by up to 40%. The change in cavity allows tuning the lasing envelope for a maximum range of 10 nm. That means the surface tensions induced a wavelength shift of the laser.

2.1.4. Liquid Crystal Droplet Lasers

Liquid crystals (LCs) are a typical kind of soft-matter that has applications in a wide variety of optical devices ranging from liquid crystal displays (LCDs) to LC lasers.^[44,68] However, these devices are generally larger than the ones mentioned so far. In order to produce microoptical components, LC is needed to confine in micrometer scale structures like microdroplets.^[69] One of the simplest ways to get LC droplets is to embed LCs in another nonmiscible liquid or solid matrix. LC microdroplets have recently attracted a great deal of interest thanks to their applications as tunable laser sources,^[70,71] white laser systems,^[72] laser-based displays,^[73] and surfactant sensing.^[74] Figure 4d–j demonstrates an exciting example of LC droplet lasers—the first ever 3D microlasers.^[75] In this work, dye-doped cholesteric liquid crystal (CLC) microdroplets with size from 15 to $50 \mu\text{m}$ in diameter were created in glycerol by simply mechanically mixing these two materials. As they are immiscible, CLC droplets are formed spontaneously. Furthermore, due to the chirality of the CLC, a strong modulation of the refractive index is created from the center of the microsphere

to the surface in all possible radial directions. Consequently, the laser emission should be in all directions. This effect is very different from common WGM lasers where the light is confined in a plane or 2D. Figure 4d shows the microscope image of a typical CLC droplet. Due to the modulation of the refractive index, the periodic structure in the radial direction is visible (Figure 4e,f). The droplet was irradiated with a focus pulsed laser beam from a 532 nm Q-switched laser. Figure 4g–i shows the laser emission originated from the center of the droplet and is observed as a bright spot. The spot expanded with the increase of pumping energy and its intensity increases sharply above the lasing threshold. Single mode emission at a wavelength of 615 nm was obtained, which is in the long wavelength of the photonic bandgap (Figure 4j). The spectral linewidth is 0.1 nm, corresponding to Q factor of about 6.2×10^3 . This value is comparable to many other WGM droplet lasers. These 3D microlasers are potential for many applications such as optical imaging, holography, and sensing.

2.1.5. Droplet Lasers in a Microfluidic Channel

Generally, air is the environment surrounding all kind of droplets that were discussed. Due to a high refractive index contrast between droplets and the air, these droplets have excellent optical confinement, and thus lasing threshold can be low. However, these droplet lasers also suffer from some drawbacks such as uncontrollable droplet size, instability, short lifetime (due to evaporation), and difficulty in handling. These

disadvantages can be overcome if an immiscible liquid replaces the surrounded air. In 2007, this idea was first realized by Kennedy's group.^[76] In this work, the microfabricated channel with T-junction configuration was fabricated for droplet generation. Initially, the fast oil flow breaks the dispersed water–glycerol phase (70% glycerol and 30% water in weight) to small plugs in the oil. Later, the water–glycerol plugs form individual spherical droplets due to their surface tension. As a result, droplets with a diameter of about 50 μm were obtained into an oil phase in the microchannel. Refractive index of the droplets was 1.428, which was 0.135 higher compared with the oil, sufficient for WGM laser generation. This research provides a useful technique to produce uniform droplets with the possibility of tuning their size.

Following Kennedy's group, many exciting findings have been reported such as switchable microfluidic droplet lasers,^[77] multicolor microfluidic droplet lasers,^[78] and magnetically transportable microlasers.^[79] Figure 5a shows the production of magnetically water-in-oil-in-water double-emulsion droplets using a glass capillary microfluidic setup. The innermost phase was prepared by mixing Fe_3O_4 magnetic nanoparticles into polyvinyl alcohol (PVA) aqueous solution. The middle oil phase was dye-doped cholesteric liquid crystal (DDCLC). The continuous phase was PVA solution. As DDCLC and water are immiscible, double-emulsion droplets were formed. Lasing emission from the droplets was obtained under optical pumping (a Q-switched frequency-doubled Nd:YAG pulsed laser with the emitting wavelength of 532 nm). Interestingly, the movement of droplets can be controlled under a magnetic field thanks to the magnetic

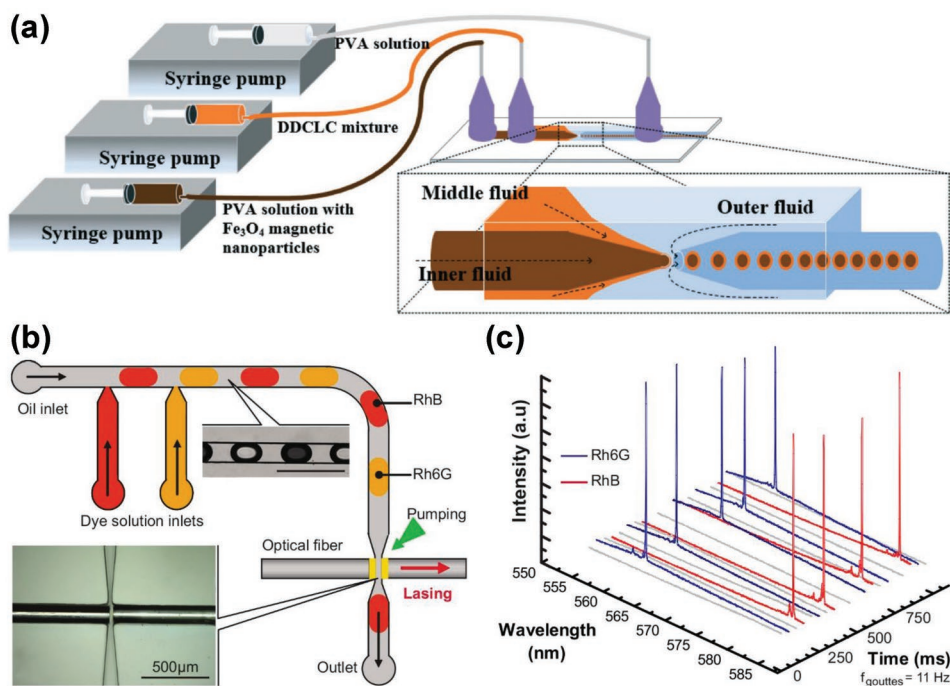


Figure 5. a) Schematic layout of a microfluidic setup for producing water-in-oil-in-water double-emulsion droplets. Reproduced with permission.^[79] Copyright 2016, Royal Society of Chemistry. b) Schematic diagram of the microfluidic device and with two droplet generators. The top inset shows the image of a train of glycol droplets in FC40 oil. The scale bar is 500 μm . The bottom inset presents the FP cavity embedded in polydimethylsiloxane (PDMS) layer. c) Time-dependence of emission spectra of the microfluidic dye laser when a stream of Rh6G/RhB droplets passes through the FP cavity. Reproduced with permission.^[80] Copyright 2011, AIP Publishing.

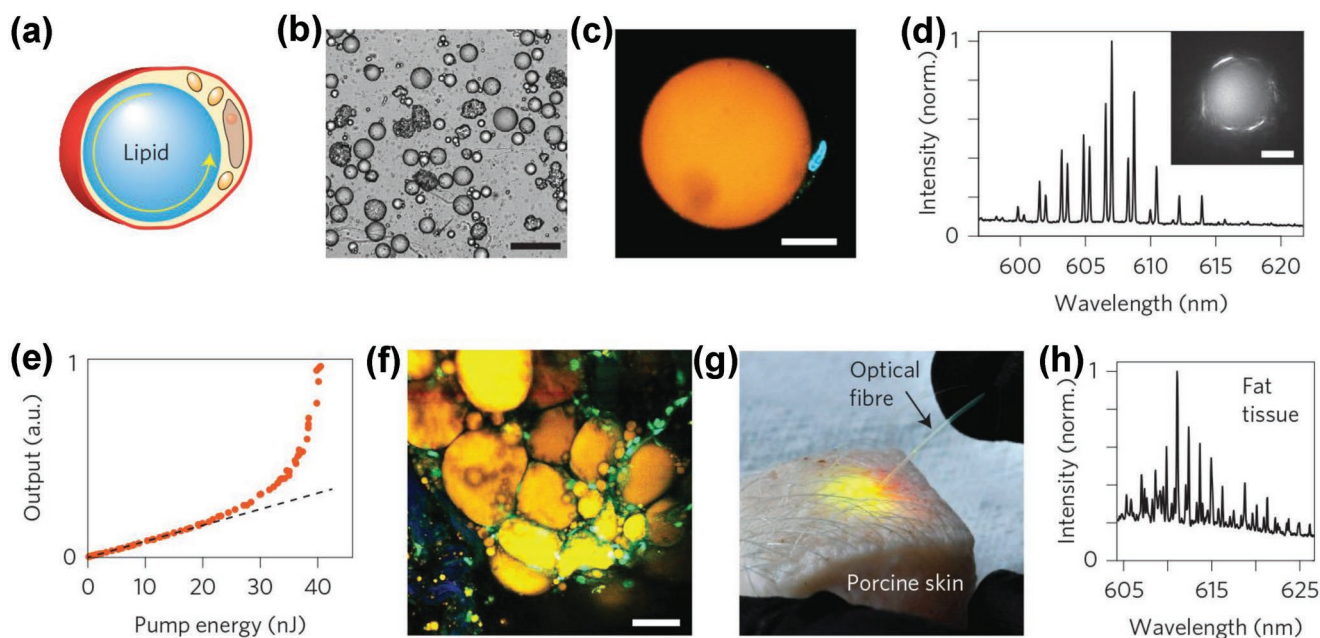


Figure 6. a) Illustration of a lipid droplet inside a single cell. b) Individual adipocytes extracted from subcutaneous porcine fat. c) Confocal image of an adipocyte showing the cell volume is mostly occupied by a large lipid droplet (orange). The nucleus (blue) is visible at the edge of the droplet. d) The emission spectrum of a 45 μm adipocyte showing a typical WGM multimodes. The inset presents the fluorescence image of the corresponding cell while it is irradiated above the lasing threshold. e) The output energy of the droplet versus various pump energies. f) Confocal fluorescence image of adipocytes in situ in subcutaneous fat tissue, after injection of Nile red dye (yellow) and pumped by a pulsed green laser. g) Laser emission from within tissue is observed upon optical excitation using the optical fiber. h) Lasing spectrum obtained from the tissue via the optical fiber. Scale bars, 200 μm (b) and 20 μm (c), (d), (f). Reproduced with permission.^[45] Copyright 2015, Springer Nature.

nanoparticles embedded inside the droplets, which may be potential for in-channel illumination applications

Generally, droplet lasers rely on droplet cavities and the light amplification via WGMs. However, in a few cases, a droplet does not serve as an optical resonator, but an external cavity does (Figure 5b).^[80] A microfluidic channel with two T-junctions (placed in series) was used to generate glycol droplets. This particular design allows obtaining continuous streams of one dye droplet or an alternation of two dye droplets, which supports either one color or multicolor lasing. For laser generation, an external cavity made of two cleaved gold-coated fibers is placed downstream beside the channel. Figure 5c plots the lasing spectra recorded as a function of time when two dye droplet stream passes through the cavity. Apparently, the lasing wavelength can be switched in time. The switching frequency can be up to kHz. A wavelength on-demand laser may be possible by using preloaded cartridges that contain different lasing media.^[81] It has been demonstrated that microfluidic channels are an excellent tool for droplet generation. A combination of microfluidics and droplet lasers is promising for wavelength tuning, biosensing, and on-chip sensing applications.

2.1.6. Intracellular Microlasers

As discussed, above microdroplets embedded in a fluid medium can support laser oscillation if the refractive index of the droplets is higher than that of the outside medium. That means a droplet in any environment (liquid or solid) may

support lasing if the condition of refractive index contrast is satisfied. Definitely, droplet lasers embedded in elastomer were reported.^[24,82] Recently, researchers have pushed it even further by showing lasing emission in biological samples such as tissues and cells, opening the new path for intracellular biosensing, cell tagging, and cell tracking.^[45,46,83] **Figure 6** shows intracellular lasers based on natural lipid droplets existed in adipocyte cells.^[45] The illustration of a lipid droplet in an adipocyte cell is shown in Figure 6a. These droplets are naturally existent in fresh adipocytes (Figure 6b). After incorporating a lipophilic fluorescent dye into the lipid droplets by incubation and pumping with a pulsed laser, the cells exhibited WGM lasing (Figure 6c,d). The output energy versus input pumping shows a distinct threshold of about 30 nJ (Figure 6e). Furthermore, generating lasing from adipocytes in situ in tissues is also possible but requires much higher pumping energy, because the adipocytes in fat are nonspherical in shape (Figure 6f), so the optical losses are relatively high. To solve this issue, the authors injected a mixture of collagenase and lipophilic Nile red dye into the subcutaneous fat and spherical shapes were acquired. An optical fibre was used to guide the pulsed laser to excite the adipocytes and the emission is collected by the same fiber (Figure 6g). The emission spectrum is plotted in Figure 6h, confirming that lasing is readily observed from adipocytes in situ in tissues. As droplet lasers are very sensitive to the surrounding medium, they can be employed for in situ sensing. Research into this field demonstrates that laser implantation for bioimaging and biosensing applications may be available in the near future.

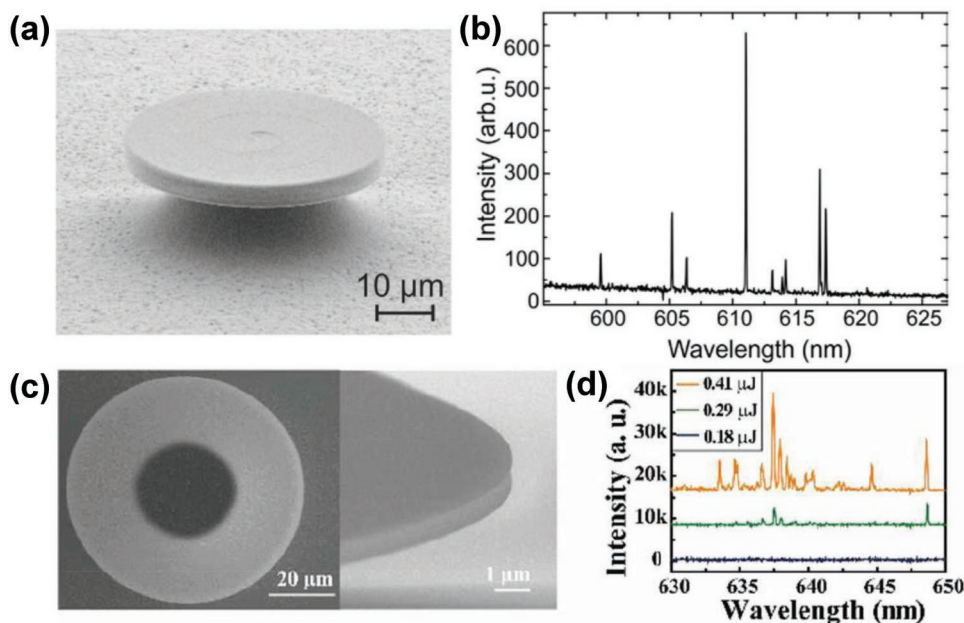


Figure 7. a) Scanning electron microscope image of a polymer microdisk fabricated by direct laser writing. b) Spectrum above the lasing threshold from the microdisk. The spectral linewidth is about 0.062 nm. Reproduced with permission.^[98] Copyright 2011, Optical Society of America. c) Top-view and side-view SEM image of a dye-doped SU8 microdisk. d) Emission spectra from the microdisk under different optical energy. Reproduced with permission.^[99] Copyright 2018, Royal Society of Chemistry.

2.2. Soft-Matter Microlasers Developed from Polymers

Compared with liquid droplet lasers, solid-state lasers are different in several respects: they are more stable (their shape and size are less affected by external environment) and easier to handle. In many cases, they can be produced in a more controlled fashion and with much more possible shapes than droplets. As a result, solid-state microlasers generally provide great flexibility in terms of breath of potential materials, cavity geometries, and applications. Polymers are a type of soft-matter that has been widely used for solid-state lasers.

Shortly after the discovery of liquid droplet lasers, polymer solid-state microsphere lasers were investigated.^[84,85] Due to the chemical flexibility, polymer materials can be easily formed into different configurations such as micro-hemispheres,^[86] microdisks,^[87] microfibers,^[88] conical microcavity,^[89] and especially a significant number of DFB structures.^[90–97] In most of the works, polymers are used as host materials, except conjugated polymers.^[25] Below, we will discuss polymer lasers based on various cavity configurations including microrings, microdisks, microhemispheres, microfibers, and nanofibers. After that, organic semiconductor lasers will be examined in a separate section.

2.2.1. Microring and Microdisk Lasers

One of the pioneering works on polymer microlasers, a microring laser, was developed by Kuwata-Gonokami et al.^[87] The microring was formed by dipping a standard glass fiber in a dye-doped polymer solution, allowing the polymer droplet to coat a thin layer on the fiber by surface tension. Under optical

pumping, WGM lasing was observed from the microring structure. Recently, a variety of flexible methods have been adapted to fabricate polymer microlasers (will be discussed in more detail in Section 3).^[39] **Figure 7a** shows the scanning electron microscope (SEM) image of a microdisk enabled by direct laser writing (DLW).^[98] The Q factors of above 10^6 at the wavelength of 1300 nm were recorded from the passive microdisks. By doping the resist with Pyrromethene 597 dye and pumping with a pulsed laser, WGM lasing emission at visible wavelengths was observed from active microdisks (Figure 7b). The spectral linewidth was 0.062 nm, corresponding to Q factor of laser modes or about 10^4 , which is higher compared with droplet lasers.^[64,66] Especially, a record of ultranarrow spectral linewidth of 0.008 nm was achieved from a RhB-doped SU8 microdisk laser (Figure 7c).^[99] The disk was fabricated by spin-coating and subsequently inductively coupled plasma etching. The microdisk was pumped normally on the top surface by a frequency doubled Nd:YAG nanosecond laser at the wavelength of 532 nm, repetition rate 10 Hz, and pulse duration 7 ns. The development from spontaneous emission to lasing emission can be seen in Figure 7d. The lasing threshold was relatively low, around 290 nJ.

Recently, scientists have developed a novel lasing structure based on coupled WGM cavity, which is called parity-time (PT) symmetric lasers.^[100–102] This kind of lasers have unique properties such as the ability to control the modes oscillating within a laser cavity, allowing to achieve stable single-longitudinal mode operation.^[100] Even though primarily of pioneering PT-symmetric lasers rely on semiconductor, organic materials have been already investigated and demonstrated as a promising candidate.^[103] It would be interesting to explore further soft-matter PT-symmetric lasers as flexible and cost-effective components for future photonic applications.

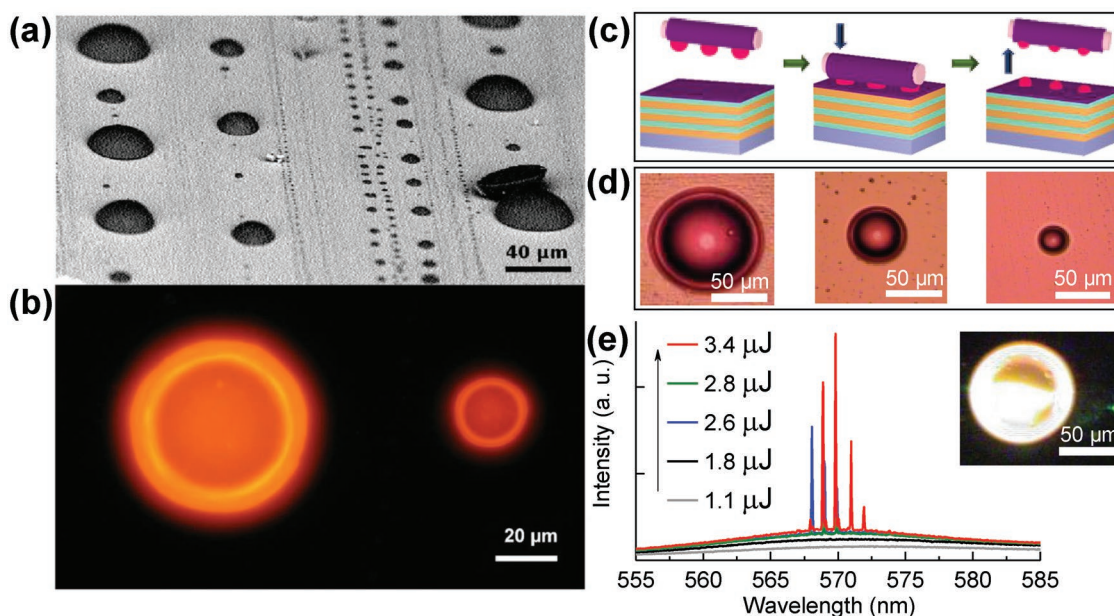


Figure 8. a) SEM image of polymer hemispheres formed on a DBR enables by hydrophobic spreading. The structures are well-aligned in rows corresponding to the spreading direction. b) Fluorescence image of the nanocrystal quantum rod-doped polymer hemispheres in (a). Reproduced with permission.^[54] Copyright 2010, AIP Publishing. c) Formation of droplets on a tip by hydrophobic spreading. These droplets are then transferred from the tip onto the hydrophobic DBR substrate. d) Top-down optical micrograph of individually fabricated hemispheres. e) Emission spectra of a typical hemisphere (its fluorescence image is shown in the inset) under various pump pulse energies. Reproduced with permission.^[86] Copyright 2012, Wiley-VCH.

2.2.2. Microhemisphere Lasers

Figure 8 presents a special kind of WGM cavities, a dome-shaped structure, the so-called hemisphere, on a distributed Bragg reflector (DBR).^[54,86] In this hybrid system, the DBR is designed to be reflective at the emission wavelength but transparent at the excitation wavelength. As a result, the emission light is still trapped inside the hemispheres in 3D like common microspheres. Interestingly, the presence of the planar DBR allows the selective excitation of different regions in the hemisphere,^[54] which is generally problematic for spherical cavities.^[104] Figure 8a shows the SEM image of polymer hemispheres formed on a DBR substrate. The samples were prepared by a technique called hydrophobic spreading.^[54] First, the DBR was cleaned and subsequently deposited with a highly hydrophobic material on top. Second, a drop of an aqueous solution that contains a water-soluble polymer and emitters (CdSe/CdS core/shell nanorods) was dropped on the hydrophobic DBR, followed by spreading it over the surface. Owing to the surface and interfacial tension forces, thousands of microdroplets were formed spontaneously. Finally, the obtained droplets were heated until dry. The droplets shrink (due to water evaporation) originating structures that are segments of spheres rather than hemispheres. However, they can be called hemispheres because they can work as WGM cavities. Figure 8b presents fluorescence microscope images of two typical hemispheres, indicating visible bright rings at the circumference of the two structures. Like droplet lasers, this is the evidence of WGMs. Further analysis has confirmed the existence of WGMs in the form of fluorescence rather than lasing (probably the excitation has not reached the lasing threshold).

Inspired by the above work, Sun's group attempted to realize lasing emission from hemispherical structures.^[86] They discovered a low-cost and commercially available material (Araldite 506 from Sigma-Aldrich) that is well suited for producing high-quality hemispheres. The fabrication technique was also modified for better control of the size and position of the hemispheres (Figure 8c), allowing to produce hemispheres with sizes from around 5–100 μm. Selective hemispheres with a variety of sizes are shown in Figure 8d. They possess a round shape and a visible smooth outer surface that are essential for the good optical confinement. When pumping with a pulsed laser, lasing emission was observed from the hemispheres. Figure 8e plots the emission spectra from a single 80 μm diameter hemisphere as a function of pumping energy. The evolution from spontaneous emission (broadened spectrum) to lasing emission (sharp peaks) is visible. The lasing threshold was about 2.5 μJ. The spectral linewidth of lasing mode was ≈0.9 nm, corresponding to a Q factor of ≈ 6×10^3 . The Q factor is higher compared to microdroplet lasers. Based on this achievement, Sun's group developed more fascinating methods to obtain hemispheres with precise control of their size and position using a microplotter system.^[105] Furthermore, promising applications based on these microstructures were also studied such as single mode lasers,^[106] chemical vapor sensing,^[107] green quantum dot laser,^[108] and fluorescence-based temperature sensors.^[109]

2.2.3. Microfiber and Nanofiber Lasers

Among many microstructures, polymer micro/nanofibers are low-cost and flexible building blocks for micromechanics,

electronics, and photonics.^[110,111] Active polymer fibers can support laser oscillation using different configurations.^[112] In 2009, Camposo et al. reported laser emission from poly(methyl methacrylate) (PMMA) electrospun polymer nanofibers.^[88] The laser was based on a small piece of fiber and their two end facets served as reflectors (a kind of FP cavity) for light amplification. Similar work has been carried on dye-doped PS fibers but the authors found that the light was not only travelling in the axial direction but also transversely.^[113] Interestingly, grating structures can be directly patterned on a single fiber to obtain DFB lasers.^[114] In addition, as polymer fibers can possess a circular cross-section thus Ta et al. were able to utilize WGM polymer fiber lasers.^[115,116] Additionally, as polymer fibers are mechanically flexible, they can form several configurations like ring and knot structures. Thanks to the waveguiding effect, this geometry can guide light sufficiently to a closed loop for laser oscillation.^[117–120] Polymer fibers can also form a network for random lasers.^[121–127] Below, we will examine typical structures.

Figure 9a demonstrates self-coupling resonators made of dye-doped polymer nanowire and their typical lasing emission (Figure 9b).^[118] The fiber can form different loop structures

for light amplification. Under pulsed excitation, single mode laser was obtained. The lasing wavelength can be slightly tuned by adjusting the diameter of the fibers or the loop structure. An alternative approach for single-mode generation is based on a coupled cavity. In this coupled structure, lasing wavelengths that satisfy the resonance condition for both fibers are enhanced while others are suppressed. As a result, the number of lasing modes reduces significantly, and single mode emission can be easily obtained. This phenomenon is called the Vernier effect.^[128] Ta et al. demonstrated that single mode emission could be obtained from a coupled polymer fiber structure (Figure 9c).^[115] The coupled structure consisted of two individual fibers that were in contact (as shown the inset of Figure 9c). The individual fiber emitted multiple WGM lasing modes under optical excitation. However, thanks to the Vernier effect, single mode emission was obtained from the coupled fiber. The spectral linewidth of lasing mode is 0.09 nm, comparable to that of single fibers. That means while the Vernier effect provides single mode emission, it does not significantly affect the *Q* factor of the lasing mode. This work highlights the possibility of integrating between polymer

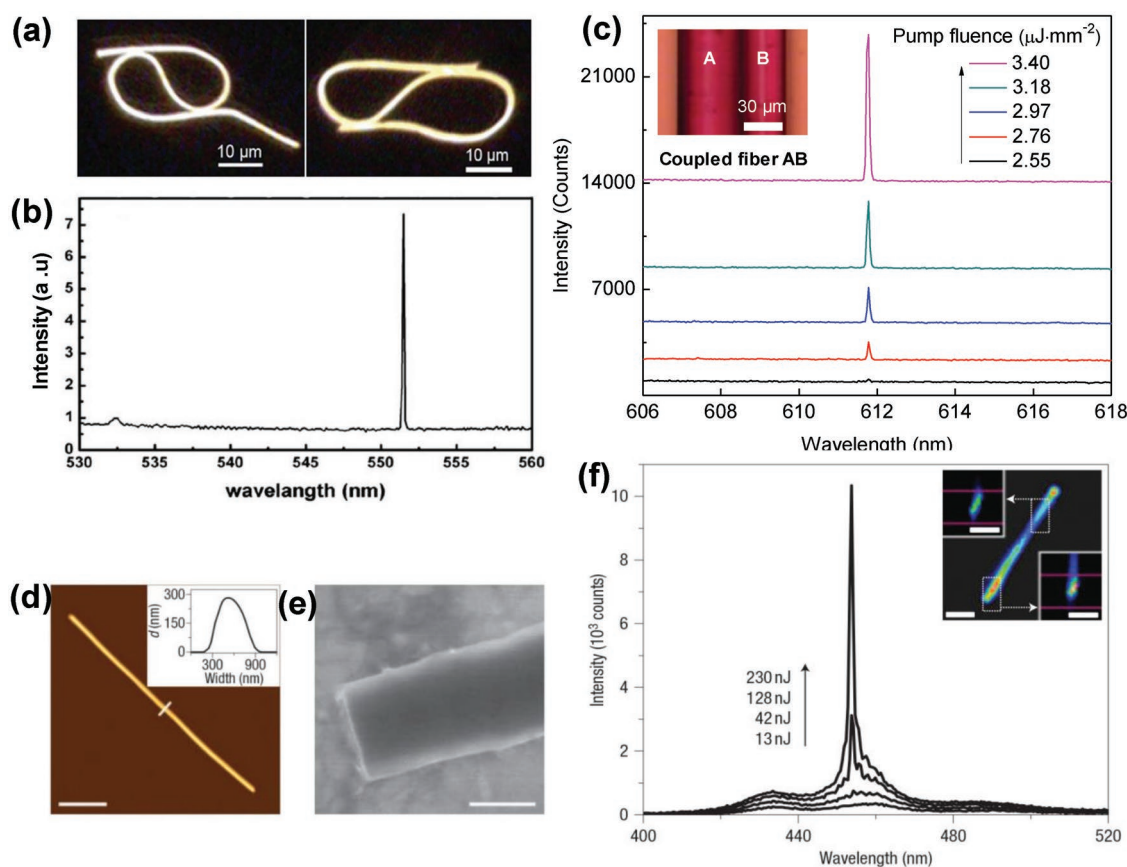


Figure 9. a) Fluorescence microscope images of self-coupling resonators. b) The single-mode lasing from a typical self-coupling fiber at a fluence of 66.4 mJ cm⁻². Reproduced with permission.^[118] Copyright 2013, RSC Pub. c) Fluorescence spectra of a coupled polymer fiber versus various pump fluences. The inset shows an optical microscope image of the studied structure. Reproduced with permission.^[115] Copyright 2014, Wiley-VCH. d) AFM micrograph of a single polymer wire on a glass substrate. Topography line profile measured across the wire at the indicated position is shown in the inset. e) High-resolution SEM image of a nanowire end facet. f) Emission spectra of a single PFO nanowire under various pump energies at room temperature. The inset shows the fluorescence image of the wire under pump energy of 1.3 nJ. Scale bars are 2 μm. Reproduced with permission.^[139] Copyright 2007, Springer Nature.

fibers for better lasing performance, which represents a step forward to all polymer fibers-based optical devices.^[129]

2.2.4. Organic Semiconductor Microlasers

It has been demonstrated that polymer materials can serve as flexible resonator structures for light amplification. In particular, conjugated polymers^[130] are a special case, as they emit light under optical or even electrical pump. As a result, the laser can be generated directly from conjugated polymer structures without the need of doping active medium. In 1992, the first organic semiconductor laser was reported.^[131] Since then various resonator configurations have been investigated for lasers with improved lasing performances. For instance, in 1996, scientists at Cavendish laboratory successfully realized lasing emission from poly(*p*-phenylenevinylene) using a traditional FP cavity.^[132] Conjugated polymer lasers have been demonstrated in microring,^[133] DFB,^[134–137] nanowires,^[138,139] microspheres,^[140] hemispherical open microcavities,^[141] and toroidal microcavities.^[142] Figure 9d,e shows respectively atomic force microscope (AFM) and SEM images of a single conjugated polymer nanowire.^[139] Due to the flat end faces, the nanowire can act as a FP cavity. With optical pumping, lasing emission is observed (Figure 9f). The lasing threshold was quite low, only about 100 nJ.

Conducting polymers are promising for electrically pumped lasers due to their capability of charge transport. Electrically pumped lasers are more compact, and therefore, more attractive in comparison with traditional optically pumped devices. A significant research effort has been devoted to the realization of electrically pumped polymer lasers. In 2008, Yang et al. demonstrated indirect electrically pumped lasing in a hybrid polymer laser.^[143] In this work, a fabricated polymer DFB laser was placed in contact with an InGaN light-emitting diode (LED). The LED was served as an optical pump source for the polymer lasers. Single mode lasing at 568 nm was observed for peak drive currents above 144 A. In 2011, Tsiminis et al. achieved LED pumped polymer lasers by using similar configuration but with a new gain medium.^[144] The pump threshold was significantly reduced to 770 W cm⁻², which is reached by mass-produced LEDs. In 2014, Dawson's group reported highly photostable, mechanically flexible, laser diode pumped polymer DFB laser encapsulated by glass membranes.^[145] By bending the ultrathin glass structure, the polymer laser was wavelength-tunable between 535 and 545 nm. Very recently, organic semiconductor lasers operating in the quasi-continuous-wave regime have been demonstrated.^[146] The utilization of semiconducting conjugated polymer lasers, primarily operating in the continuous-wave regime, is a critical step toward the realization of optoelectronic devices based on these fascinating materials.

2.3. Soft-Matter Microlasers Developed from Biomaterials

The use of biological materials in laser devices started in the early 1970s. In 1977, chlorophyll (the principal photoreceptors for photosynthesis in green plants and bacteria) lasers were first

reported. Biomaterials used as host cavity were investigated even earlier. In 1971, Hansch et al. reported dye lasers in gelatin.^[147] Since fluorescein (the dye used as a gain medium) is nearly nontoxic, these lasers were probably the first ever edible. In the same year, the first DFB lasers based on gelatin were reported.^[148]

2.3.1. Whispering Gallery Mode Cavity Based Biolasers

WGM biolasers are attracting a great deal of interest for their potential as future biocompatible sensors with enhanced sensitivity. Particularly, optofluidic biolasers have been widely employed for bioanalysis at the molecular level.^[149–152] Figure 10a shows schematically the first human whole blood lasers based on a high *Q*-factor optofluidic ring resonator.^[153] In this structure, a thin capillary tube served as a resonator for laser generation. Blood with the gain medium (indocyanine green) flows to the tube. The whole structure is optically pumped in the vertical direction, perpendicular to the axis. As the capillary has a circular cross-section, it supports WGMs like a ring resonator. Lasing spectra at three different pump fluences are plotted in Figure 10b.^[153] The observation of optofluidic lasers using FDA approved laser material makes them promising for clinical and biomedical applications. Owing to biocompatibility, miniature biolasers may be integrated into single cells and tissues for cell-tracking and in situ sensing.^[45] Using simple emulsion effects and with green processes, Ta et al. demonstrated that solid microspheres made from bovine serum albumin (BSA) protein and polysaccharides (derived from plants) can be fabricated.^[154] By doping organic dyes into these structures and pumped with a pulsed laser, lasing emission was observed. Figure 10c presents a BSA microsphere surrounded by many HeLa cells.^[154] There was no inhibition area surrounding the laser particle. Also, it was found that the presence of BSA spheres did not prevent cell growth and division, giving basic evidence of the laser biocompatibility. Lasing emission from the fluorescein doped BSA microsphere is plotted in Figure 10d, indicating WGM properties. Furthermore, it was found that the lasing mode and intensity of an individual sphere maintain nearly the same values after immersing in water for 22 h, indicating the stability of the laser. WGM lasing has also been achieved in BSA microdisks.^[155] Lasing from starch microspheres^[156] and slab planar waveguides of the lysozyme amyloid fibrils^[157] were also reported. Additionally, poly(lactic-co-glycolic acid) (PLGA) and poly(lactic acid) (PLA) (both are approved for medical use) have been employed for laser resonators. WGM lasing from within tissues and whole blood based on microspheres was realized (Figure 10e–g).^[158] These implanted lasers are potential applications to real-time biosensing.

2.3.2. Distributed Feedback Cavity Based Biolasers

Biolasers have been also obtained from DFB configurations. Toffanin et al. demonstrated blue lasing from a stilbene doped silk film spin-coated onto a 1D DFB grating.^[159] Similarly, Choi et al. reported a single-mode DFB laser in the form

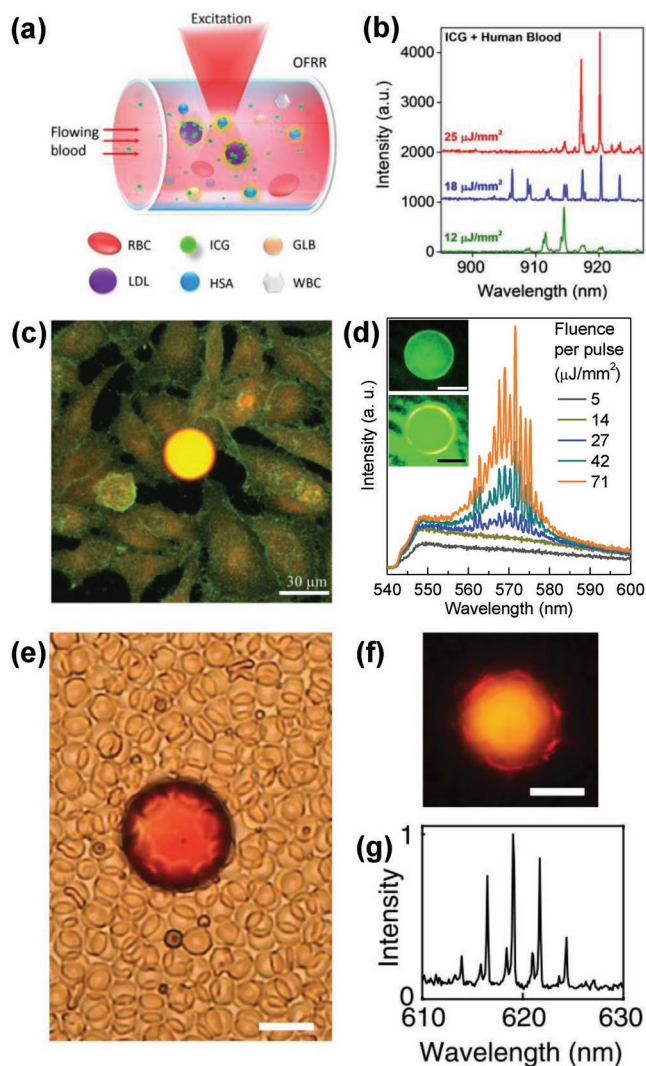


Figure 10. a) Illustration of an optofluidic biolaser. RBC, red blood cell; ICG, Indocyanine green; GLB, globulin; LDL, low-density lipoproteins; HAS, human serum albumin; WBC, white blood cell (leukocytes). b) “Blood” lasing spectra under different pump fluences. The ICG concentration was 0.04×10^{-3} M. Reproduced with permission.^[153] Copyright 2016, Optical Society of America. c) A 30 μm diameter BSA microsphere in a culture medium. The sphere is surrounded by HeLa cells. d) Emission spectra of a fluorescein doped BSA microsphere under various pump fluences. Reproduced under the terms of the Creative Commons Attribution License.^[154] e) A 40 μm diameter PLA microsphere in blood. The sphere is surrounded by blood cells. f) Fluorescence microscope image of the same PLA bead in blood and g) its lasing spectrum. Scale bars are 20 μm . Reproduced with permission.^[158] Copyright 2017, Optical Society of America.

of a free-standing film that consists of silk, riboflavin, and silver.^[160] Vannahme et al. demonstrated single-mode DFB lasers made of riboflavin (vitamin B2) doped gelatin films on nanostructured low refractive index material (Figure 11a).^[161] In this work, the fabrication was based on simple nanoimprint and spin coating. As shown in Figure 11b, the laser emitted at wavelengths of 543 and 562 nm corresponds to two different grating periods.

2.3.3. Random Media Based Biolasers

Compared with conventional lasers, random lasers are cheap and easy to fabricate, as they rely on disordered structures to trap light.^[162] Recently, random lasers have attracted a great deal of interest due to their rich physical properties^[163] and potential applications for cheap light sources,^[164] unidirectional high intensity and high Q factor lasing,^[165] and speckle-free laser imaging.^[166,167] Random lasing has been achieved in biological tissues,^[168–170] cellulose,^[171,172] silk,^[173] and other biomaterial structures.^[174,175] Figure 11c,d shows the SEM image of silk inverted photonic glass and lasing emission from it, respectively.^[173] This structure provides strong scattering at emission wavelengths of the gain medium, which supports random lasing. The porous structure was produced using solution-processing with two main steps. First, PS nanospheres and silk were mixed to form a photonic glass. Then the PS spheres were selectively removed by chemical etching. As the laser worked in the diffusive regime, the lasing spectrum was quite broad, and sharp peaks were not visible. Random lasing based on biological materials/structures is potential for a number of applications such as effective tools for separating malignant from healthy tissues,^[169] probing nanoscale structural alterations in bone,^[170] pH,^[173] and dopamine sensing.^[176]

2.3.4. Fabry–Perot Cavity Based Biolasers

Even though lasing can be achieved in a variety of configurations including biological structures, it is surprising to see lasing emission in something that is alive. Remarkably, Gather and Yun successfully realized biolasers based on living cells in 2011.^[177] First, the authors studied green fluorescent protein (GFP) purified from bacterial culture and found that GFP was a practical gain medium for optical amplification. Then, a living enhanced GFP (eGFP)-expressing 293ETN cell was embedded between two highly reflective DBRs for laser generation (Figure 12a). Under optical pumping, fluorescence emission was visible from the cell (Figure 12b). At pump energy of 0.9 nJ, single mode lasing appeared, and additional emission lines were generated at higher pump energy (Figure 12c). The lasing threshold was less than 1 nJ per pulse, which was ultralow and may be reached by a diode pulsed laser. Following this success, the authors demonstrated lasing emission from *E. coli* bacteria using a similar experimental setup (Figure 12d–f).^[178] Inspired by this work, lasing amplification was also investigated from live *E. coli* bacterial cells suspended in aqueous droplets (Figure 3e,f).^[66] These interesting works confirm that lasing emission can be generated in biological samples despite their intrinsic high scattering and high absorption loss. The finding establishes a new route of in vivo light amplification for bioimaging and biosensing.

2.4. Soft-Matter Microlasers: Typical and Novel Materials

As discussed in the previous sections, materials play essential roles in cavity design, emitting wavelength, and lasing properties in any laser device. Below, we examine typical and novel soft-matters that are attractive for microlasers.

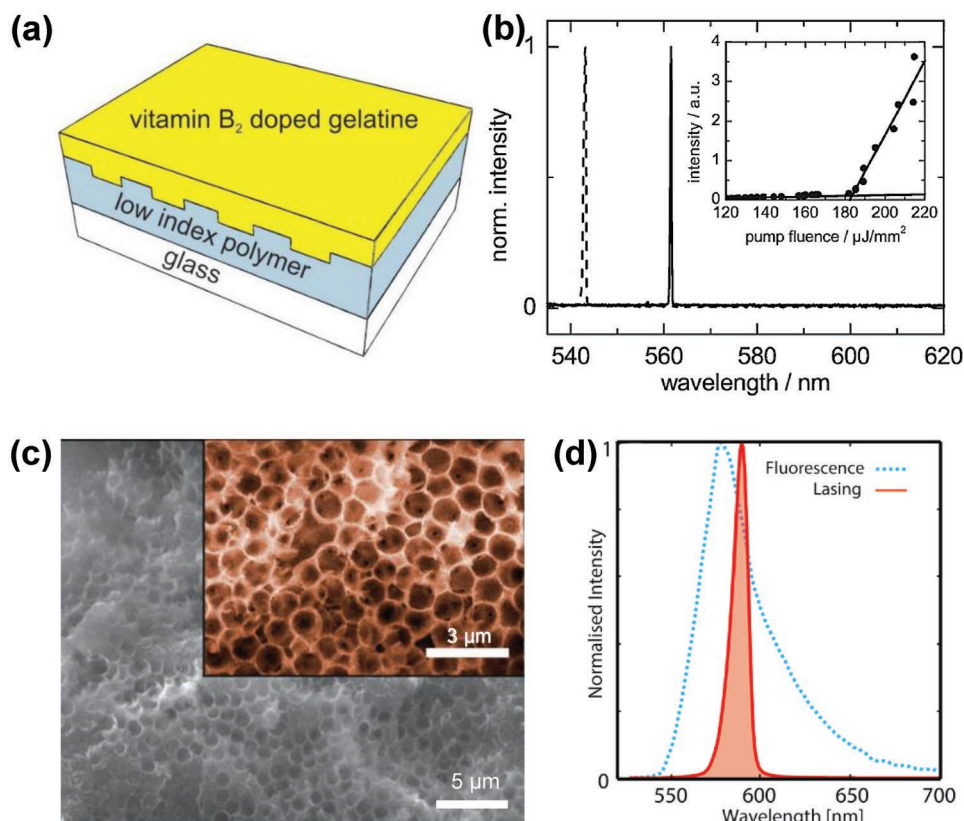


Figure 11. a) Illustration of biological DFB laser. b) Normalized lasing spectra obtained from DFB lasers with two different periods, 368 nm (dashed) and 384 nm (solid), respectively. The inset plots laser output energy of a DFB laser as a function of the pump fluence. Reproduced with permission.^[161] Copyright 2013, Royal Society of Chemistry. c) SEM image of silk inverted photonic glass. The inset shows the close-up image of the air voids and the silk structure. d) Spectra showing fluorescence and random lasing emission. Reproduced under the terms of a Creative Commons Attribution License.^[173] Copyright 2016, The Authors.

2.4.1. Active Media

Among a great deal of available gain media, semiconducting (conjugated) polymers are attractive for solid-state lasers.^[179] **Figure 13a** shows three major groups of polymers that have been studied for laser generation.^[25] There are several reasons driving the research into polymer lasers:^[25] i) They can cover the whole visible spectrum as shown in **Figure 13b**; ii) They are promising for suitable for tunable lasers owing to their broad emission; iii) They can have high-efficiency thanks to their strong absorption coefficients; iv) They are not affected by the reabsorption effect as their absorption and emission are well separated; (v) They can be used to make electrically pumped lasers. Recently, the demonstration of polymer lasers pumped by LEDs^[143,144] and laser diodes^[145] is a critical step toward electrically pumped polymer lasers.

Recently, biocompatible and biodegradable optical gain media based on biologically produced materials have attracted extensive research due to their potential in implantable photonic devices.^[180,181] Chlorophyll, a pigment that gives plants green color and is responsible for the process of photosynthesis is the biomaterial that was investigated as laser dye a long time ago. In 1977, the first observation of chlorophyll lasers was reported.^[182] This finding was further developed by Far's group by using isolated chlorophyll a (Chla) to make efficient WGM

optofluidic lasers.^[183] Another biomaterial is Luciferin—a light-emitting compound found in many organisms generating bioluminescence which can also serve as a gain medium. In 2013, Fan's group again achieved optofluidic lasers with luciferin.^[184] Especially, GFPs is the most well-known biomaterial for lasers.^[185] In 2002, Pikaš et al. found that GFP can work as a laser dye.^[186] Later, eGFPs were used for biolasers based on living organisms (single cells and bacteria shown previously in **Figure 12**).^[177,178] Recently, GFPs have been investigated for solid-state lasers using various resonator geometries.^[187–189] Interestingly, an exciton–polariton laser based on eGFPs has been realized.^[190] The finding demonstrates the efficiency of eGFP as an active optical material. Other types of active biomaterial are molecules derived from vitamins. **Figure 13c** shows a chemical structure of vitamin B2 (riboflavin) in the form of flavin mononucleotide (FMN).^[64] The typical absorption and emission spectra of FMN are plotted in **Figure 13d**. Riboflavin has demonstrated as a practical laser material and was used for all-biomaterial droplet lasers^[64] and DFB lasers.^[161]

2.4.2. Cavity Matrix

A great number of polymer materials have been applied as cavity matrices for laser generation. Among them, PS is an

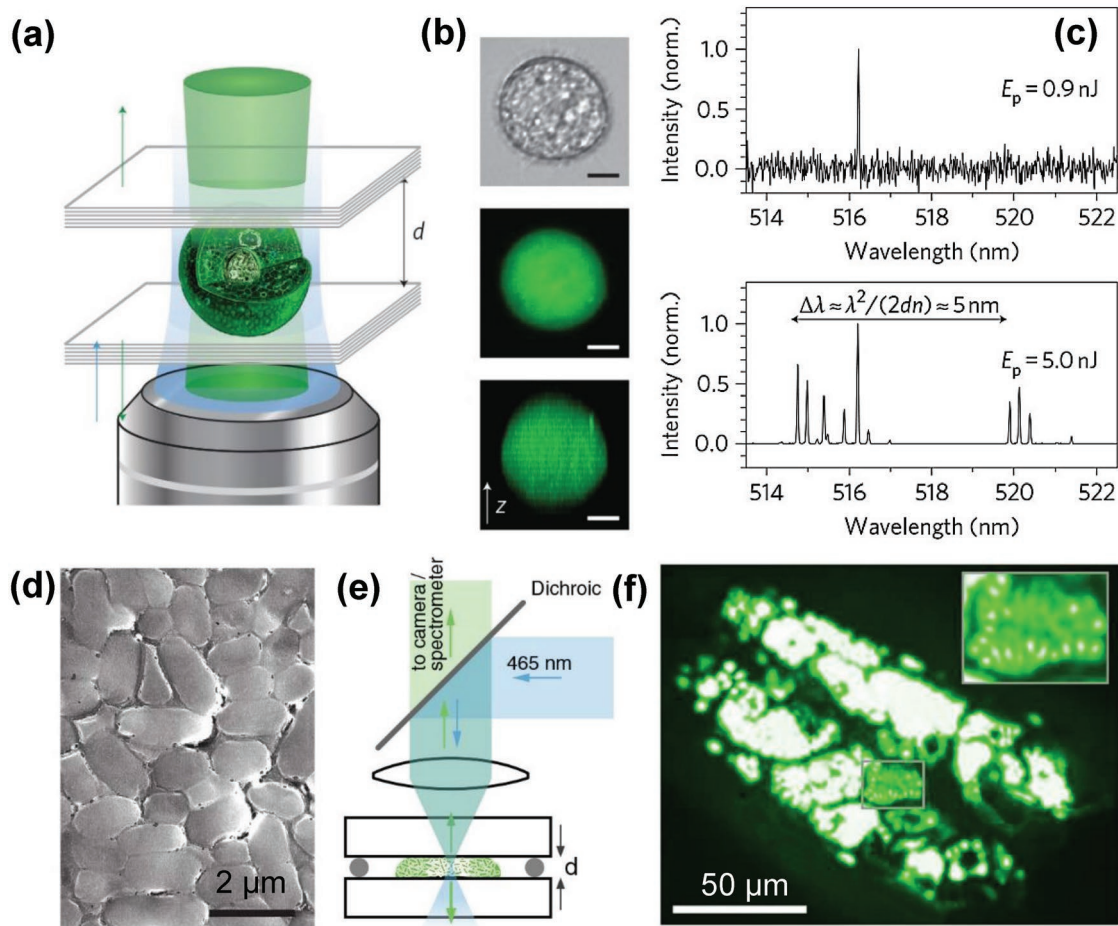


Figure 12. a) Illustration of the single-cell biological laser. A live 293ETN cell is placed inside a FP resonator ($d = 20 \mu\text{m}$). b) Microscope image, confocal fluorescence microscope image, and side-view projection of a z-stack of a confocal fluorescence image of a 293ETN. The scale bars are 5 μm . c) Normalized lasing spectra from the cell under two pump energies of 0.9 and 5 nJ, respectively. The arrow represents the expected longitudinal mode spacing. Reproduced with permission.^[177] Copyright 2011, Springer Nature. d) SEM image of a group of GFP-expressing *Escherichia coli* (*E. coli*) bacteria. e) Schematic of the optical setup for utilization of bacteria laser ($d = 18 \mu\text{m}$). f) Emission pattern of bacteria laser pumped at 3 \times its threshold. The inset is a close-up of the central area. Reproduced with permission.^[178] Copyright 2011, Optical Society of America.

attractive material for cavity matrix owing to its high refractive index ($n = 1.59$ at a visible wavelength), high transparency, and low cost. Since 1980, PS microspheres were studied for generation of WGMs.^[49] Lasing emission was reported from dye-doped PS microspheres in the early 1980s.^[191] PS microspheres offer high Q factor, enabling low-threshold microlasers with a diameter as small as 10 μm .^[192] Recently, PS microspheres were integrated into single cells for intracellular lasers.^[45,46] Another interesting polymer is PMMA known as acrylic glass.^[193] The chemical structure of PMMA is shown in Figure 14a. It is a transparent dielectric material with a refractive index of 1.49 at a visible wavelength.^[194] PMMA is widely used for active polymer fibers^[110] and also WGM microcavities.^[195,196]

LCs is a class soft-matter that combines fluid-like behavior with crystalline-like solid ordering that has been used for a wide range of optical application.^[197–201] Depending on their degree of orientational and positional order, LCs can be classified into different mesophases such as chiral nematic, chiral smectic, and blue phase (Figure 14b).^[44] One of the great properties of LCs is the large tunability with the electric field, making them

an attractive candidate for electrically tunable lasers.^[42] Furthermore, the temperature tunability of LCs is also high, allowing to get a large shift of the lasing wavelength based on a little variation of temperature.^[71] Especially, LCs droplet lasers are potentially for laser-based display applications (will be discussed in Section 4.4).^[73]

Biomaterials based matrix have been investigated a long time ago. In 1971, laser action of dyes in gelatin was reported.^[147] This achievement opened a new research field in science called biophotonics. Recent research has explored a great number of novel attractive biomaterials for laser matrices including silk protein, artificially obtained amyloids, polysaccharides, nucleic acids, tissues, and cells.^[181]

Silk, an ancient material, is emerging as a promising candidate for optics and biophotonics applications owing to its high transparency, high aqueous solubility, biodegradability, biocompatibility, and implantability.^[202–204] Among many forms, silk fibroin, derived from *Bombyx mori* cocoons, is the most popular and well-studied protein for a wide range of medical applications.^[205] Figure 14c illustrates optical-grade

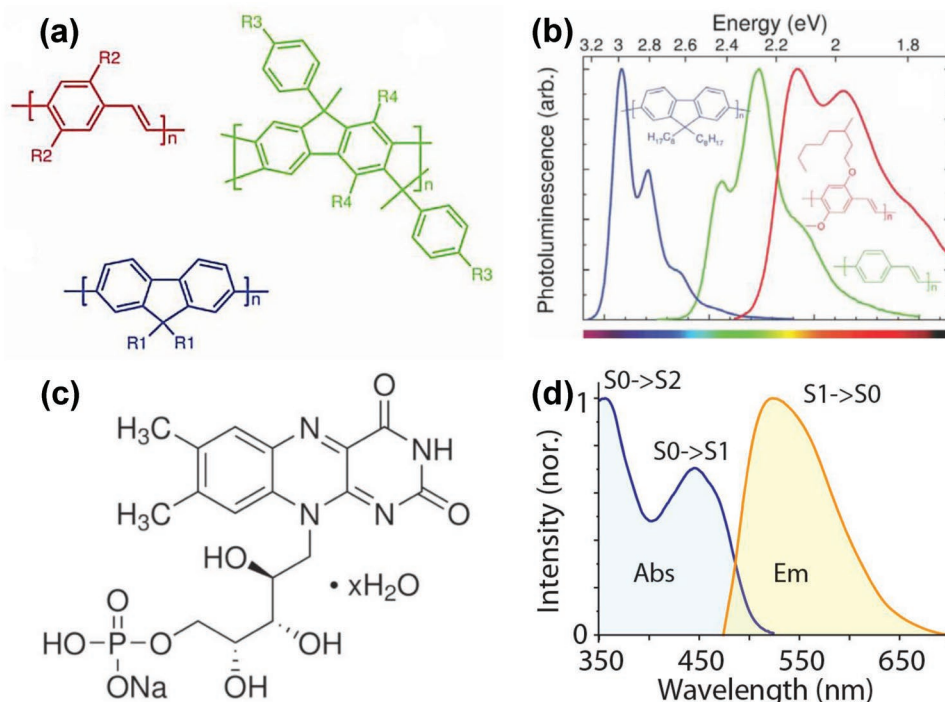


Figure 13. a) Chemical structures of conjugated polymers commonly used for lasers (from left to right and bottom): poly(phenylenevinylene)s, ladder-type poly(paraphenylene), and polyfluorenes, where R_1 , R_2 , R_3 , and R_4 denote alkyl or alkoxy groups. b) Normalized emission spectra of three popular conjugated polymers. Corresponding chemical structures are inset. Reproduced with permission.^[25] Copyright 2004, Elsevier. c) Chemical structure of flavin mononucleotide, riboflavin 5-monophosphate sodium salt hydrate and d) its absorption and emission spectra (10×10^{-6} M solution). Reproduced with permission.^[64] Copyright 2013, Wiley-VCH.

silk solution synthesized from silk cocoons.^[206] Several silk-based optical components such as waveguides,^[207,208] inverse opal,^[206] biostructural color mimicking,^[209] and high

Q factor resonators^[210] have been reported. Especially, as silk fibroin is dissolved in water, organic dyes can be easily incorporated for active photonic components. Silk-based lasers

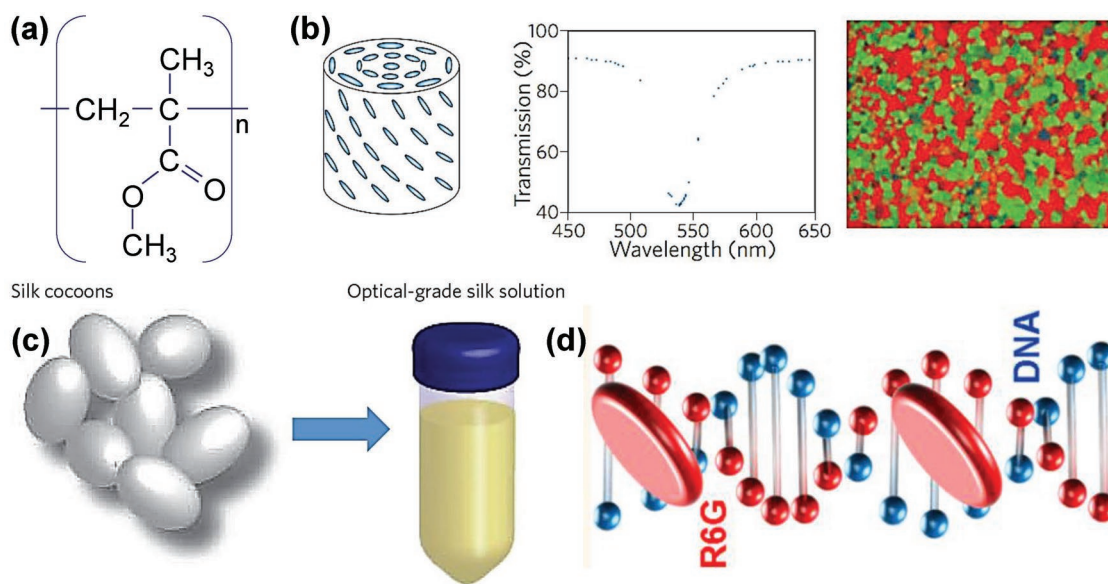


Figure 14. a) Chemical structure of PMMA. b) The configuration of the local director for blue phase liquid crystal (left), the corresponding transmission spectrum for white light (middle), and the microscope image of the optical texture captured when the sample is between crossed polarizers (right). Reproduced with permission.^[44] Copyright 2010, Springer Nature. c) Optical-grade silk fibroin solution is achieved from the cocoons of the *B. mori* silkworm. Reproduced with permission.^[206] Copyright 2012, Springer Nature. d) Schematic illustration of R6G binding to DNA helix (right). Reproduced with permission.^[221] Copyright 2014, American Chemical Society.

with various configurations have been reported, such as DFB lasers,^[159,211] and random lasers in inverse photonic glass structures.^[173] Very recently, silk fibroin-based microdisk lasers were achieved by suppressing the coffee ring effect.^[212]

Another interesting biomaterial is DNA—the molecule of life, which has been demonstrated as promising photonic material due to its biocompatibility, high transmission at visible and near-infrared wavelengths.^[213] To obtain active components, a gain medium is needed to incorporate to the DNA. It can be provided by either simple mixing of DNA with luminescent molecules or binding luminescent molecules to DNA helix. In the early 2000s, Ogata's group was one of the pioneers who attempted to utilize DNA based lasers and observed amplified spontaneous emission from dye-doped DNA films.^[214,215] Following these works, DNA films with various laser dyes including sulforhodamine,^[216] 4-(dicyanomethylene)-2-methyl-6-(4-dimethylaminostyryl)-4H-pyran,^[217] R6G,^[218,219] were investigated. In 2010, Mysliwiec et al. realized DNA based DFB lasers.^[220] In this work, a layer of a modified DNA polymer matrix containing R6G laser dye was superimposed on a grating structure formed in a photochromic polymer. The active layer was prepared from DNA mixed with cationic surfactant molecule cetyltrimethyl-ammonium chloride and R6G. The structure was excited with a pulsed laser (wavelength of 532 nm). Above the threshold of 1.8 mJ cm^{-2} , lasing emission at around 590 nm was observed. Other exciting DFB lasers were based on the binding of R6G into pure DNA helix (Figure 14d).^[221] In this work, the samples were prepared by solution-processing and nanoimprinting. Furthermore, as the architectures of the DFB lasers can dissolve in water, they could observe the physical transient from DFB lasers to random lasers.

3. Soft-Matter Microlasers: Fabrication Technologies

Most conventional semiconductor microlasers rely on either top-down or bottom-up techniques.^[222] For the top-down approach, a microstructure can be obtained by etching or patterning a planar structure.^[223] This method offers mass production of highly uniform microlasers, despite this fabrication requires costly apparatus (lithograph for patterning), sophisticated epitaxial growth techniques, and material choice (due to the requirement of lattice-matching for epitaxy). In comparison, microstructures enabled by the bottom-up approach are directly formed by self-assembled crystallization of semiconductor materials.^[224,225] For this method, precisely controlling the size and position of self-assembled structures is a challenging task. By contrast, owing to chemical and mechanical flexibility, the use of soft-matter materials would provide an alternative and cost-effective strategy to produce lasers with flexible cavity design and wavelength tunability.^[5] Furthermore, novel fabrication techniques such as imprint lithography and molding,^[226] inkjet printing,^[227] and direct laser writing^[228] are expected to enhance performances of soft-matter-based optical devices. In this section, we examine several attractive soft technologies, including self-assembling technique, solution printing technique, direct laser writing technique, electrospinning, and

direct drawing technique for fabrication of soft-matter microlasers. These technologies could produce high Q factor microlasers with much lower cost (one of the key challenges in the field) compared with using conventional semiconductor micro/nanofabrication.

3.1. Self-Assembling Technique

A variety of complex micro/nanophotonic structures can be formed by self-assembly in solution.^[229] In the self-assembled process, the interfacial tension and the hydrophobic environment play important roles.^[29] Indeed, surface tension induced droplets on superhydrophobic substrates and in microfluidic channels are good examples.^[60,76] The interfacial tension also allows for producing solid microsphere lasers via emulsion.^[154,158] For instance, Ta et al. obtained BSA, pectin, cellulose microspheres after solidifying these droplets in polydimethylsiloxane (PDMS) base.^[154] Yun's group fabricated PLA and PLGA microspheres using the standard oil in water dispersion procedure.^[158] Below, we discuss several microlaser configurations enabled by self-assembled technique.

Figure 15a,b shows what happened inside a colloidal quantum dot (CQD)/PMMA droplet when drying.^[230] Initially, tiny microbubbles appeared at the contact line of the droplet and a substrate. Then, these bubbles merged together to form larger microbubbles and moved toward the droplet center due to the solvent evaporation. As shown in Figure 15c, the bubbles possess a thin wall with a circular cross-section. As a result, they support WGMs like ring cavities. The bubbles were employed for multicolor (blue, green, red corresponding to different CQD doping) lasing emission. The Q factor of lasing modes was around 2.5×10^3 . As the gain medium was well protected by the PMMA matrix, these microbubble lasers still worked well, with almost the same lasing properties, after storing at ambient conditions for over a year. This stability is sufficient for practical uses in optical devices. Figure 15d shows another approach by which PS microdisks are produced.^[231] First, PS molecules were dissolved in *N,N*-dimethylformamide. With the addition of water, the PS molecules were forced to aggregate. Next, PS emulsion was obtained by using ultrasonic treatment. After that, two glass substrates were used to squash the spherical micelles into disk-shaped structures. Finally, PS microdisks were obtained when the solvent was completely evaporated. By doping organic dyes into these microdisks, optically pumped lasing emission was obtained. Figure 15e presents the self-assembled process that occurred on a substrate in ambient conditions rather than in a solution.^[107] Immediately after fabrication, a direct drawing polymer was gently placed on a hydrophobic DBR surface. Due to the hydrophobic layer underneath and strong interfacial tension of the material used, the fiber broke down to a number of similar small pieces after several minutes. The shape of these pieces changed over time and finally became circular. When incorporating organic dyes such as RhB into these hemispheres, WGM lasing emission was obtained upon optical pumping. Thanks to the relatively smooth outer surface and high refractive index contrast, Q factor of lasing modes was relatively high, about 10^4 for $\approx 50 \text{ }\mu\text{m}$ diameter hemispheres.

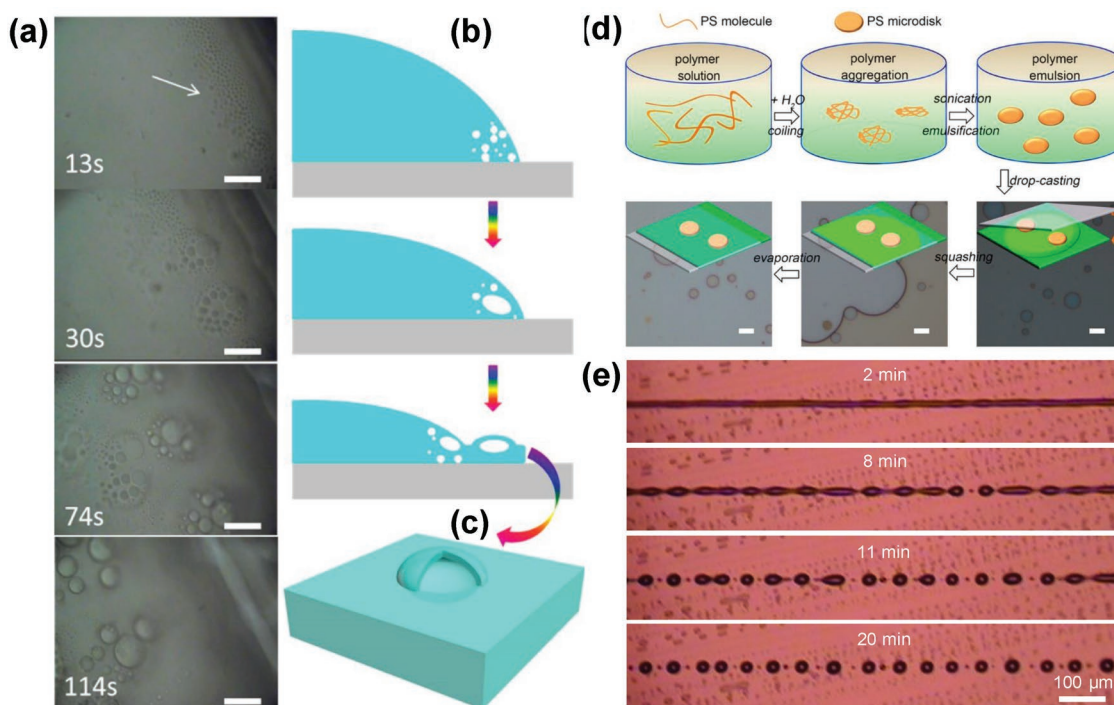


Figure 15. a) Microscope images of a CdZnS/ZnS CQD/PMMA (41 wt%) nanocomposite droplet during the drying process. The white arrow shows the position where bubbles start to appear. The scale bars are 50 μm . b) Schematic diagram explains the formation of microbubbles. c) Schematic structure of a single microbubble obtained after the drying process is completed. Reproduced with permission.^[230] Copyright 2017, American Chemical Society. d) Illustration of the microdisk fabrication process. Reproduced with permission.^[231] Copyright 2015, American Chemical Society. e) Microscope images of the self-assembled process that breaks a polymer fiber into many hemispheres. Recording time started when the fiber was placed on the substrate. Reproduced with permission.^[107] Copyright 2013, AIP Publishing.

It has been demonstrated that even though self-assembled microstructures provide excellent optical confinement for light amplification, the size and position of obtained structures are not well controlled. This disadvantage may hinder them for practical applications in optical devices. This drawback, however, can be overcome by novel techniques such as ink-jet printing and direct laser writing that is introduced in the next section.

3.2. Solution Printing Technique

Solution printing, especially by inkjet, is an attractive bottom-up microfabrication technology for flexible photonics due to its simplicity and cost-effectiveness.^[232] Recently, Zhao's group reported polymer microring cavities and lasers on a flexible chip using ink-jet printing.^[233] Particularly, the Q factor of printed passive cavities was 4×10^5 , which is at the same level of silicon-based resonators. Other types of lasers such as WGM lasers,^[234] DFB lasers,^[235] LC lasers,^[236] and random lasers^[237] can also be achieved by inkjet printing approaches. **Figure 16a** shows microlaser arrays fabricated by solution printing via a microplotter.^[105] First, the DBR substrate was coated with a hydrophobic material that helps to reduce the adhesion of the substrate and printed materials. Then, hemisphere arrays were produced using the GIX Microplotter II from Sonoplot, INC. The size and position of an individual hemisphere can be

well controlled (**Figure 16b**), which is advantageous compared to self-assembled structures. Using the same above apparatus, Wang et al. could fabricate high Q factor quasitoroid microcavities for the CQD-based lasers.^[238] The result demonstrates the advantage and flexibility of solution-printing technique for the mass production of soft-matter lasers with well-control of cavity size and shape. Another effective approach for making high Q polymer microcavities was developed by Wienhold et al.^[195] This technique relies on a series of fabrication processes including spin-coating, optical lithography, wet chemical etching, and thermal reflow. It is expected that with the rapid development of solution printing techniques, more complex photonic microstructures can be manufactured for practical devices.

3.3. Direct Laser Writing Technique

DLW has demonstrated the ability to fabricate complex nanoscale structures.^[239] Optical and photonic components such as 3D photonic crystals,^[240] multilens objectives,^[241] and WGM resonators^[242] were realized by DLW. **Figure 16c** illustrates a typical process of DLW used to fabricate polymer microdisks.^[98] The polymer used was a negative-tone photoresist Ormocomp (Micro Resist Technology). This material provides high optical transparency in both the visible and infra-red spectral region. A drop of the resist was embedded

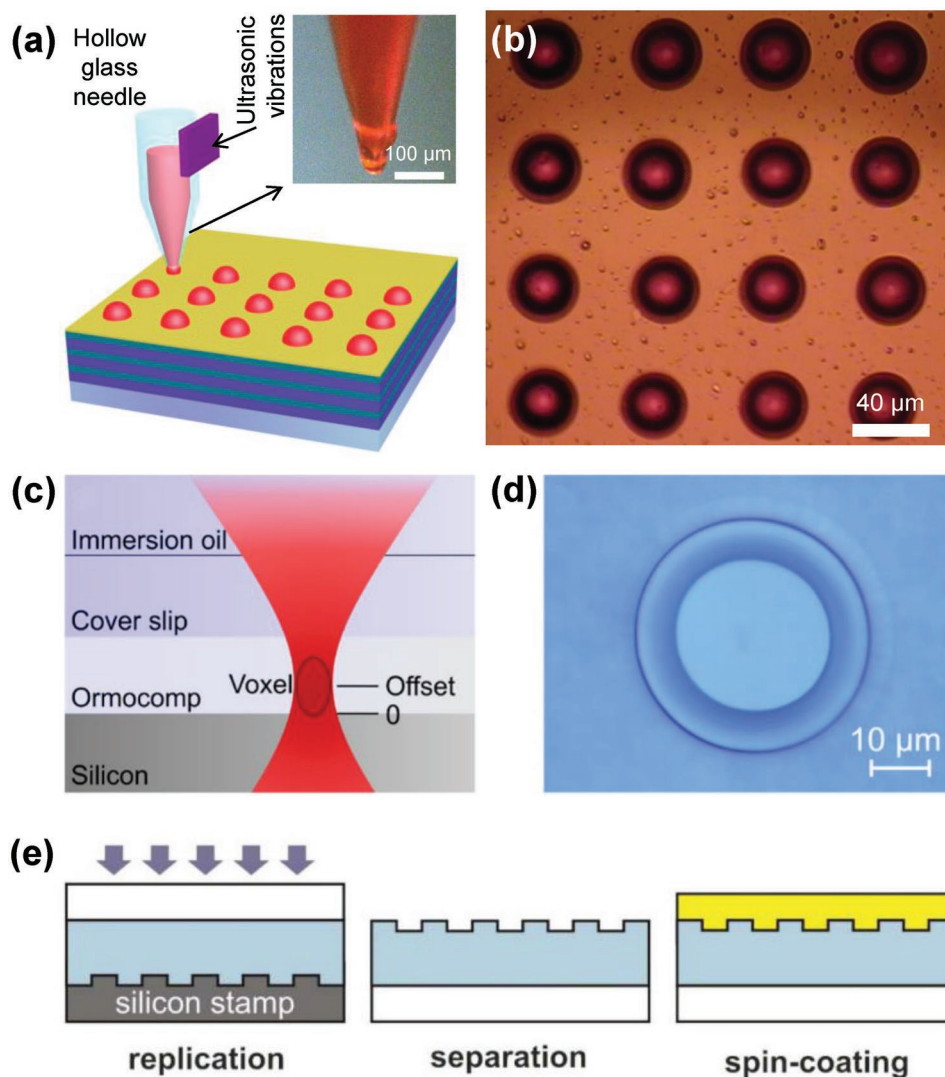


Figure 16. a) Illustration shows the fabrication of hemisphere microlasers on top of a DBR substrate using a microplotter. b) Optical microscope image of typically fabricated hemispheres. Reproduced with permission.^[105] Copyright 2015, AIP Publishing. c) Direct laser writing technique used to fabricate Ormocomp microdisks on a silicon substrate. d) Top-down microscope image of a fabricated microdisk. Reproduced with permission.^[98] Copyright 2011, Optical Society of America. e) Schematic diagram of the fabrication process of a DFB laser. Reproduced with permission.^[161] Copyright 2013, Royal Society of Chemistry.

between a glass coverslip and a silicon substrate. A commercial DLW system is equipped with a femtosecond fiber laser (wavelength of 780 nm, pulse duration below 150 fs, repetition rate of 100 MHz) for the exposure of the photoresist. The laser beam was focused onto the resist by a high magnification objective (numerical aperture NA = 1.4, 100 \times). After exposure, the coverslip was removed. Then, the sample was developed in methyl isobutyl ketone for 5 min, followed by rinsing with isopropanol. Finally, free-standing microdisks on silicon (Figure 16d) were obtained after isotropically etching the silicon by XeF₂. This procedure was used for passive resonators. By doping the Pyrromethene 597 laser dye into the resist and using the same above process, microdisk lasers would be obtained. Remarkably, the protein-BSA has been reported as a suitable material for DLW and BSA microdisk lasers have been

formed via this technique.^[243] Apparently, DLW is potential for 3D integrated photonic circuits and complex photonic systems.

3.4. Molding Technique

Molding is a very effective technique for manufacturing DBF lasers.^[244] Figure 16e presents a typical example of molding technique used for the fabrication of riboflavin doped gelatin DFB lasers.^[161] First, the DFB grating is structured on a silicon wafer by electron beam lithography and reactive ion etching. Then, a low index polymer is deposited on a silicon stamp. As a result, the grating is replicated on the polymer. Next, the polymer is cured by UV exposure, followed by the separation. Finally, an active layer is poured on the structured polymer to form DFB

lasers. Molding takes the rewards of the advanced semiconductor nanofabrication and mechanical flexibility of polymer materials, providing an alternative method for fabrication of microlasers.

3.5. Electrospinning and Direct Drawing Technique

Among a variety of nanostructures, polymer fibers are considered a flexible and versatile candidate for functional, optical, and electronic circuits.^[88] To fabricate polymer fibers, electrospinning is an alternative approach due to low-cost and the ability to produce nanofibers of different materials in various sizes and fibrous structures.^[245–247] Figure 17a illustrates the basic principle of the electrospinning technique.^[246] Typically, it consists of three main components: a power supply, a spinneret (where fibers pass through), and a grounded collector.^[245] The spinneret is connected to a polymer solution. When a high voltage is applied, particles within the solution are charged. At a critical value, electrostatic forces can overcome the surface tension of the polymer solution, leading to ejection of a liquid jet from the tip of the spinneret. Using this simple technique, fibers with diameters from tens of nanometers to a few micrometers can be achieved. Active nanofibers have many

applications such as light sources, field-effect transistors, sensors, photodetectors, and photovoltaics.^[110,112] Figure 17b presents the fluorescence microscope image of typical active electrospinning polymer fibers.

In principle, electrospinning fibers possess a circular cross-section and therefore they can support WGM lasing. In practice, it is hard to realize WGM laser using electrospinning fibers because of their small size (generally less than 10 μm in diameter). To overcome this issue, Ta et al. fabricated fibers by direct drawing from a polymer solution (Figure 17c).^[116] The fiber's diameter can be modified by drawing speed. The use of this simple technique can produce long fibers with a diameter from 5 to 100 μm . For example, fibers with diameters around 25 and 100 μm are shown in Figure 17d. Owing to the smooth outer surface and circular cross-section, WGM lasing with the lasing threshold of ≈ 400 nJ per pulse and Q factor up to 8×10^3 were achieved from these fibers.

4. Soft-Matter Microlasers: Applications

As discussed in the introduction, microlasers are building blocks for both fundamental studies of light–matter interaction

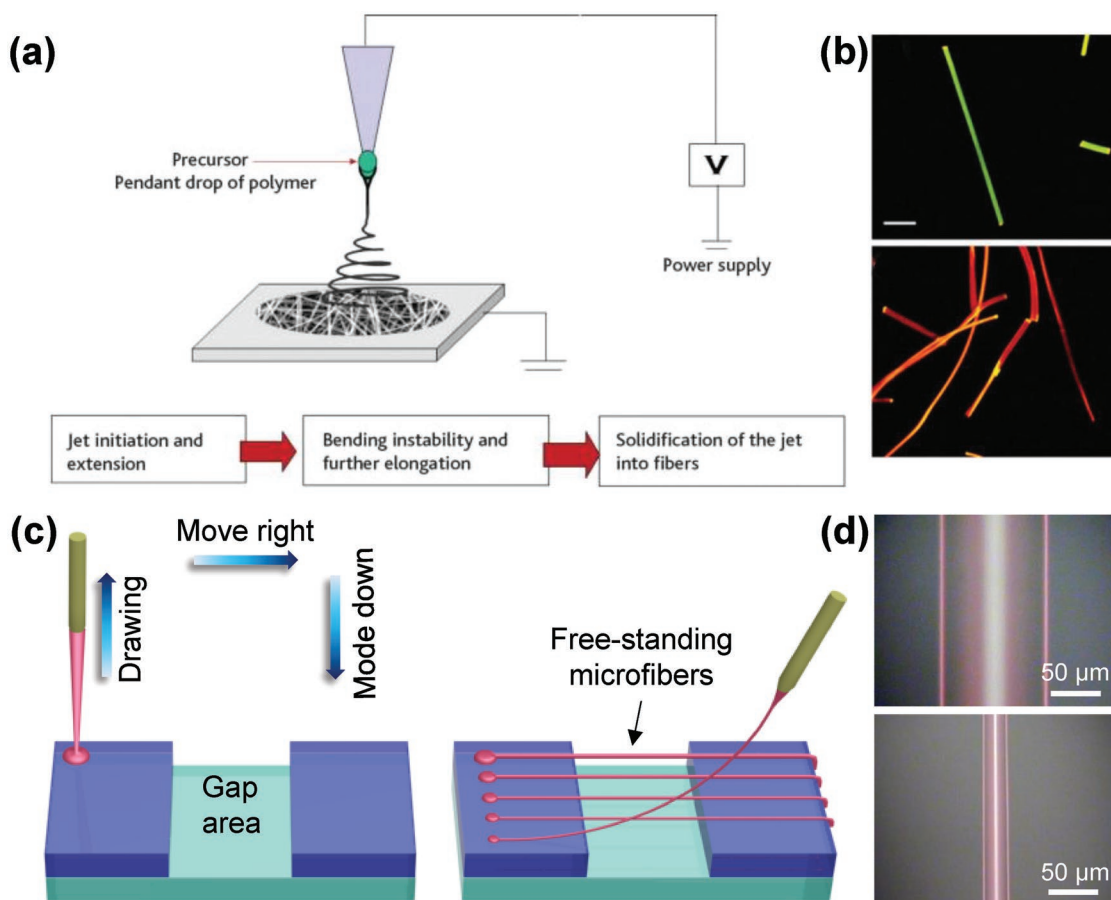


Figure 17. a) Illustration of electrospinning technique used for the fabrication of polymer fibers. Reproduced with permission.^[246] Copyright 2006, Elsevier. b) Fluorescence microscope images of electrospinning PMMA fibers with Coumarin 334 and Rhodamine 6G, respectively. The scale bar is 10 μm . Reproduced with permission.^[88] Copyright 2009, Wiley-VCH. c) Schematic diagram of direct drawing technique used to fabricate polymer microfibers. d) Microscope images of direct drawing fibers with different diameter. Reproduced with permission.^[116] Copyright 2013, Wiley-VCH.

and a variety of practical applications.^[1] For example, microlasers can be used for on-chip communications and information processing. Recently developed photonic crystal lasers with a very low operating energy of 4.4 fJ bit⁻¹^[136] and waveguide embedded plasmon nanolasers^[248] are highly potential for such applications. High *Q* factor microlasers have also demonstrated as ultrasensitive biosensors with a detection limit down to single viruses and nanoparticles (in a range of tens of nanometer).^[249] For the application mentioned above, soft-matter lasers are not comparable to their semiconductor counterparts. However, owing to chemical and mechanical flexibility, soft-matters lasers are advantageous to a certain desires such as wide range emission and wavelength tuning. With regard to the sensing, even though in some cases, the sensitivity of soft-matter lasers is not as high as passive and active semiconductor counterparts, they are convenient and well suited for numerous sensing applications. Furthermore, owing to biocompatibility and biodegradability, soft-matter biolasers are highly promising for in vitro and in vivo biosensing. In this section, we discuss the typical applications of soft-matter microlasers for wavelength-tunable light sources, biosensing and cell tracking, physical and chemical sensing, and display.

4.1. Wavelength-Tuning Applications

As mentioned previously, laser tunability is a desirable property for many applications. Tunability can be accomplished by directly modifying the gain medium, refractive index, and cavity geometry, or indirectly by external factors like electric field, temperature.^[42] In conventional semiconductor microlasers, the wavelength tunability is limited by the material bandgap and doping inflexibility. By contrast, owing to mechanical and chemical flexibility, the lasing wavelength of soft-matter lasers can be easily tuned by changing the above parameters. Based on this design, the lasing wavelength can be switched within a millisecond, opening a pathway for a selective wavelength laser on-demand. Alternatively, various gain materials can be doped into a single cavity for a wide range of lasing wavelengths. Ta et al. obtained lasing wavelength at either green, red color, or a combination of both by doping two 2 laser dyes (with a certain ratio) into a single hemisphere.^[105] Gardiner et al. demonstrated multicolor lasing (blue, green, red wavelengths) by stacking blue, green, red layers of LC droplets into a single structure.^[250] Another way to tune the lasing wavelength is by changing cavity size. Tang et al. studied a series of dye-doped droplet lasers with continuously decreasing radius in a microfluidic channel and has found that the lasing wavelength could change from 700 to 620 nm, as the radius of the drops decreased from 21 to 7 μm.^[251] Similarly, Yang et al. developed floating droplets with reconfigurable size and recorded a shift of 10 nm in the lasing envelope.^[67] The shape of a laser cavity can also affect the output wavelength. For example, Ta et al. observed a wavelength tuning by deformation of dye-doped droplets in a flexible PDMS elastomer.^[24]

Figure 18 illustrates electrically and mechanically tunable lasers, respectively. In both works, the wavelength tuning mechanism was based on the modification of the refractive index of the laser cavity. Figure 18a–c shows the effect of electric

field on a nematic liquid crystal (NLC) droplet embedded in a PDMS matrix.^[42] Obviously, the internal structure of the NLC in the droplet changes with increasing field that leading to variation of the refractive index of the droplet. Consequently, the lasing mode shifted to shorter wavelengths with the increase of the applied field (Figure 18d).^[42] Larger droplets exhibited better wavelength tuning and a relative wavelength shift of about 3% was recorded from a 16 μm diameter droplet. The authors claimed that tuning ranges up to 40 nm could be achieved with a proper selection of LC materials and at reasonable voltages. External temperature can also lead to shifts in lasing wavelengths.^[252] Wang et al. demonstrated a wavelength tuning of 9.1 nm within 6 °C temperature interval in a 20 μm diameter CLC microdroplet.^[71] Another way to tune the lasing wavelength is by using mechanical stress. Chen et al. fabricated dyed doped PMMA polymers embedded in a PDMS matrix (Figure 18e).^[253] When bending, the strain-induced refractive index change of the fiber, leading to the wavelength tuning (Figure 18f). Interestingly, bidirectional tuning of the laser wavelength was observed by different types of bending. Alternatively, Görrn et al. demonstrated elastically tunable DFB lasers based on stretchable PDMS gratings.^[254] Recently, Wood et al. reported wavelength-tunable (up to 40 nm) laser emission from stretchable chiral NLC gels.^[255] The development of tunable lasers may enhance the function of photonic devices such as mechanical flexibility, lightweight and open the opportunity for new sensing applications.

4.2. Biosensing and Cell Tracking Applications

Owing to the inherent high *Q* factor, WGM optical microcavities and microlasers are suitable for label-free biosensing applications.^[41,256–258] For WGM lasers, as shown in Equation (1), the resonance wavelength depends on the cavity size and the refractive index of the surrounding medium. As a result, changes in the refractive index (Δn) and the radius of the cavity (ΔR) induce shifts ($\Delta\lambda$) in resonance wavelengths that is given by^[256]

$$\frac{\Delta\lambda}{\lambda} = \frac{\Delta R}{R} + \frac{\Delta n}{n} \quad (4)$$

Where *R* and *n* are respectively the radius and refractive index of the cavity. A red shift in the WGM is observed with increases in the radius or refractive index. Based on this principle, WGM lasers have been widely used for biosensing applications (an in-depth review of this topic is already available^[41]).

The wavelength shift resulting from adsorption of molecules with excess polarizability (α_{ex}) and average surface density (σ) is given by^[259]

$$\frac{\Delta\lambda}{\lambda} = \frac{\alpha_{\text{ex}} \sigma}{\epsilon_0 (n_1^2 - n_2^2) R} \quad (5)$$

where ϵ_0 is the vacuum permittivity, n_1 and n_2 are the refractive indices of the cavity and the surrounding medium, respectively. Furthermore, the polarizability of binding molecules to the cavity surface is proportional to its weight, providing an extra

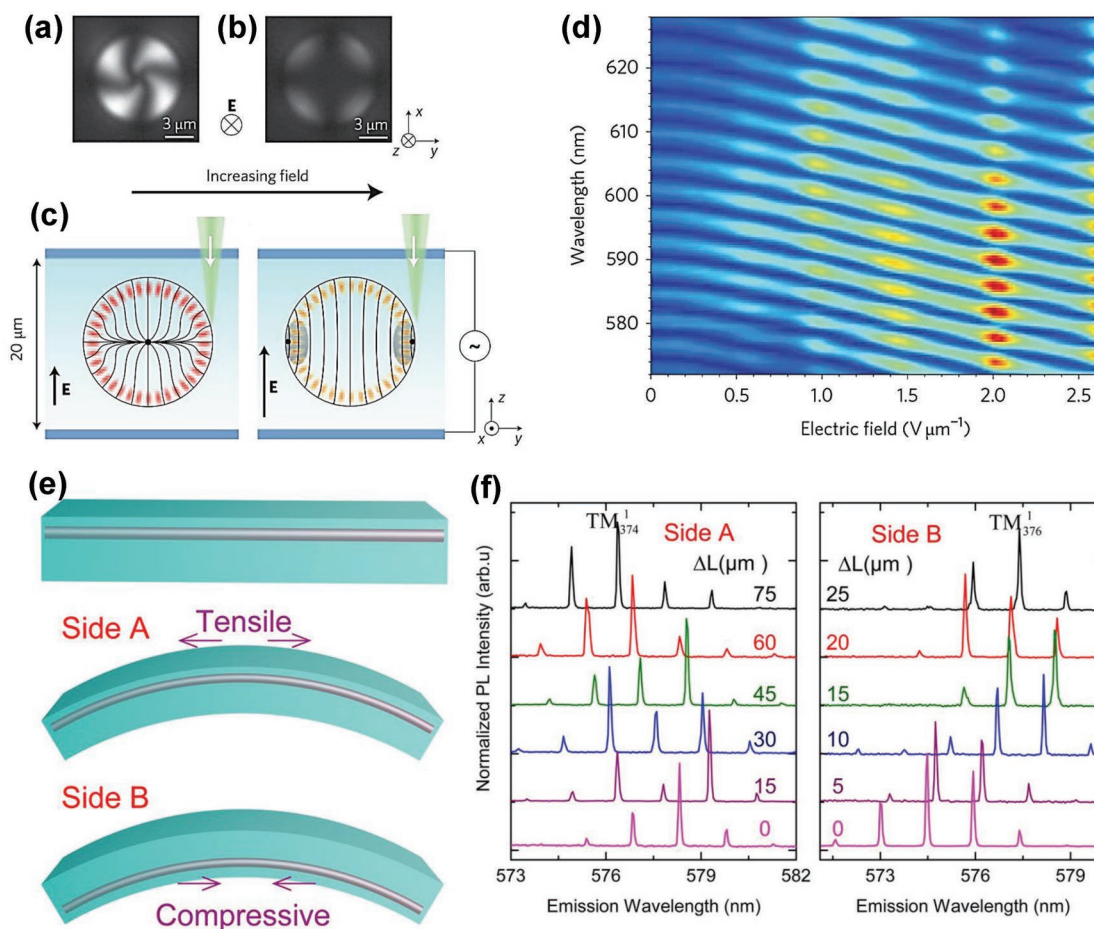


Figure 18. a,b) Microscope images through a crossed-polarizer of a 9.3 μm droplet of E12 in PDMS micrographs with increasing electric field strength. c) Illustration of the alignment of NLC molecules when applying an external electric field at two different levels. d) Wavelength shift in a 16 μm diameter dye-doped LC microdroplet. The color scale represents the output lasing intensity. Reproduced with permission.^[42] Copyright 2009, Springer Nature. e) Depiction of a dyed doped PMMA polymer fiber embedded in PDMS under mechanical bending. f) The lasing spectra from a fiber as a function of bending level. Reproduced with permission.^[253] Copyright 2014, American Chemical Society.

dimension to the WGM sensor. Indeed, Vollmer et al. could determine the mass (5.2×10^{-16} g) of a bound virion based on the optimal resonance shift of the WGM sensor.^[260]

Figure 19a,b demonstrates a special kind of in vitro biosensing based a droplet laser.^[45] The dye-doped oil droplet ($n = 1.69$) was injected into the cells and then pumped with a pulsed laser. Live cells induce internal stress, which deforms the droplet. The deformation is exhibited in the emission spectrum and can be used to determine the stress value. Experimentally, the authors observed the fluctuation of output spectra with the time that revealed the dynamic variations of the cellular stress in live cells (Figure 19a). By contrast, emission from the droplet in dead cells was entirely flattening, as there was no internal stress. Based on the baseline in the dead cells, the force sensitivity was calculated to be ≈ 20 pN μm^{-2} . The mean fluctuation of the internal stress was determined to be ≈ 150 pN μm^{-2} (Figure 19b). An additional application of intracellular microlasers is for cell tagging and tracking. Schubert et al. used the lasing spectra of microspheres embedded in cells as a barcode-type tag to identify and track individual migrating cells.^[46] Figure 19c shows the migration path of a group of cells

can be followed for 19 h. The lasing spectra from each cell have unique characteristics such as the dominant wavelength (highest intensity mode) and mode spacing (Figure 19d). These two features could be used to distinguish 41 individual cells reliably (Figure 19e). The authors estimated that about 1800 individual cells can be identified.

4.3. Physical and Chemical Sensing Applications

Based on the above principle, WGM microlasers have been exploited for sensing pressure, temperature, humidity, and chemical sensing.^[41] For example, Sun's group demonstrated strain-induced bidirectional tuning of the WGM resonances, enabling the possibility of bend sensing applications. Liu et al. performed temperature sensing using dyed-doped oil droplet immersed in aqueous solution.^[261] The temperature induced wavelength shifts giving by^[261]

$$\Delta\lambda = \lambda \left(\frac{\alpha}{n} + \beta \right) \Delta T \quad (6)$$

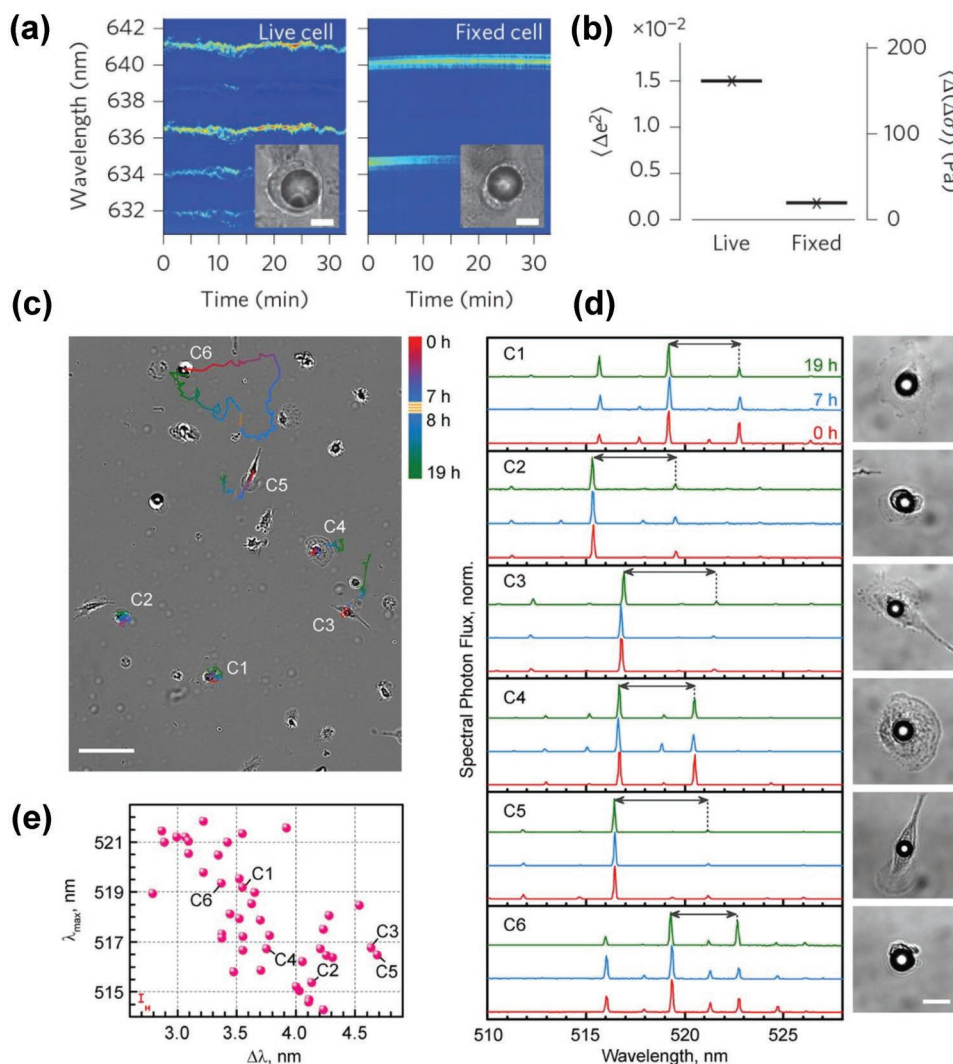


Figure 19. a) Output spectra as a function of time for a live cell (left) and a dead cell fixed with formaldehyde (right). b) Standard deviation of the square of eccentricity versus corresponding internal stress for live and fixed (dead) cells. Scale bars are 10 μm . Reproduced with permission.^[45] Copyright 2015, Springer Nature. c) Microscope image of six primary macrophage cells with embedded microspheres (labeled C1–C6). The migration path of each cell is monitored over the 19 h, and represented by the colored solid. About 7 h after the beginning of the experiment, lasing experiments were performed and indicated by orange dashed lines. Scale bar is 100 μm . d) Lasing spectra from each cell (left) and microscope images of each cell at 0 h. Arrows represent the mode spacing. Scale bar is 20 μm . e) Dominant lasing wavelength (λ_{\max}) as a function of mode spacing. Reproduced with permission.^[46] Copyright 2015, American Chemical Society.

where $\alpha = \Delta n/\Delta T$ is the thermos-optical coefficient and $\beta = \Delta R/(R\Delta T)$ is the thermal expansion coefficient, R is the radius of the microsphere resonator; n is the refractive index of the resonator; T is the ambient temperature.

The authors reported a sensitivity of 0.377 nm $^{\circ}\text{C}^{-1}$ in the temperature range 25–45 $^{\circ}\text{C}$. Similarly, Wang et al. observed temperature tunable WGM lasing in CLC microdroplet immersed in an aqueous solution (Figure 20a).^[71] Lasing modes exhibited a linear blue-shift with the increase of temperature. The sensitivity was determined to be about 1.5 nm $^{\circ}\text{C}^{-1}$, about four times better than the previous work.^[261] Very recently, Yang's group reported the use of an optical WGM microcavity in a wireless sensor for thermal sensing and aerial mapping.^[262] This work demonstrates the capability of WGM optical sensors in practical applications.

In terms of chemical sensing, microlasers have been employed for sensing surfactant, chemical solvents and vapors, pH values, etc. For example, Humar and Muševič reported the use of NLC droplets floating in water for sensing a surfactant called sodium dodecyl sulfate (SDS).^[74] The presence of SDS affects the orientation of liquid crystal molecules in the microdroplet, leading to the changes of the lasing spectrum. Based on this effect, a minimum change of 0.5×10^{-3} M of SDS could be detected. Furthermore, the effect of structural changes in LC droplets influenced by contaminants was applied for ultra-sensitive sensing with a sensitivity of 1pg mL⁻¹ of endotoxin in water.^[263] Another work also using floating droplets could sense water-soluble organic compounds such as ethanol.^[67] In this work, Yang et al. realized that the presence of ethanol in aqueous solution affects the size of floating droplets, which changes the

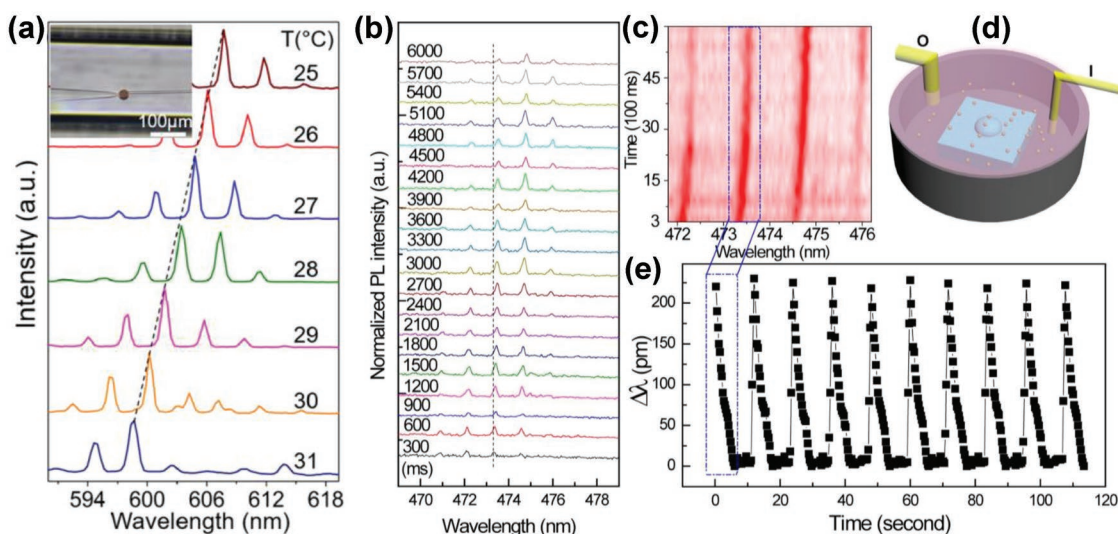


Figure 20. a) Lasing spectra of a 20 μm diameter LC droplet as a function of measured temperature. The inset shows the microscope image of the droplet. Reproduced with permission.^[71] Copyright 2016, AIP Publishing. b) Lasing wavelength shift of lasing spectra from a $\approx 31 \mu\text{m}$ diameter microbubble laser as a result of water vapor. c) Mapping of the wavelength shift with time (red color represents high intensity). d) Setup for demonstrating water vapor sensing using the microbubble laser (I: input; O: output). e) Dynamic and reversible shift of lasing peak at around 473.3 nm as a result of loading and unloading of water vapor. Reproduced with permission.^[230] Copyright 2017, American Chemical Society.

output lasing spectra. Using the FSR as an indication, a sensitivity about $20 \text{ THz}/(\text{mol mL}^{-1})$ and the detective limit around $5.6 \times 10^{-3} \text{ mol mL}^{-1}$ were obtained. Wang et al. demonstrated water vapor sensing based on CQD microbubble lasers.^[230] The authors found that the output lasing spectrum exhibited a blue-shift with the presence of water vapor (Figure 20b). All lasing modes shifted by the same value (Figure 20c). The blue-shift of the lasing modes may be due to two main factors: i) the reduction of effective refractive index of the microbubble and ii) the decrease of the size of the microbubble, both caused by the presence of water vapor. Interestingly, the lasing modes returned back to their original wavelengths when the vapor was completely unloaded. Owing to the structural robustness and high photostability, the reversible shift of the lasing peaks was highly reproducible (Figure 20e). Similarly, Ta et al. employed hemisphere dye lasers for acetone vapor sensing with an estimated sensitivity of 130 nm per refractive index.^[107]

Besides WGM structures, other configurations such as DFB lasers and random lasers are also well suited for certain sensing applications. Lu et al. demonstrated the ability to perform dynamic monitoring of surface-adsorbed mass by immersing a DFB laser in a chemical solution.^[264] The authors reported the detection of Human IgG with concentration as low as $3.4 \times 10^{-9} \text{ M}$. Alternatively, Caixeiro et al. used random lasers for pH sensing.^[173] In this work, the sensing mechanism was based on the modification of gain medium by pH. As a result, the change in lasing intensity and eventually the complete suppression of lasing (rather than the shift of lasing wavelength) are indications of the pH variation.

4.4. Display Applications

LCDs is a ubiquitous electrooptical device. As LCDs do not emit light, LCDs rely on backlight combining with inherent

light-modulating properties of LCs. In LCDs, color filters and optical polarizers are required elements. However, with the development of LC lasers, it is possible to produce laser-based displays without the use of such optical components.^[44] In 2008, Coles's group demonstrated a 2D LC laser array with specific either green or red emission.^[265] Soon after, his group developed the system further to obtain a polychromatic laser simultaneously. Figure 21a shows a schematic of the polychromatic CL laser array.^[73] The presence of a lenslet array helps to redistribute the pumping energy to excite multiple gain regions of a conventional LC cell. As a result, simultaneous red–green–blue emission is obtained in the out of the LC cell (Figure 21b). This laser array provides high spectral purity with micrometre-sized cavity length, enabling the production of a large-area projection display with excellent resolution and without using polarizers or color filters.^[44]

5. Summary and Future Prospects

Recent years have witnessed the rapid developments of soft-matter microlasers. Just a few years ago, it was impossible to imagine that something as simple as a droplet could be employed for given the advantages of microlasers. Owing to the low cost and mechanical flexibility, the soft-matter may even replace conventional semiconductor materials in certain photonic applications. For instance, even though most of the current PICs rely on semiconductor structures,^[266–270] polymer waveguides^[271] and cavities^[272] have demonstrated their ability for such applications. In addition, many new fabrication technologies have developed to enhance the performance of soft-matter-based microcavities and microlasers. Recently, microring cavities and lasers fabricated by inkjet printing technique provided high Q factors that are compatible with

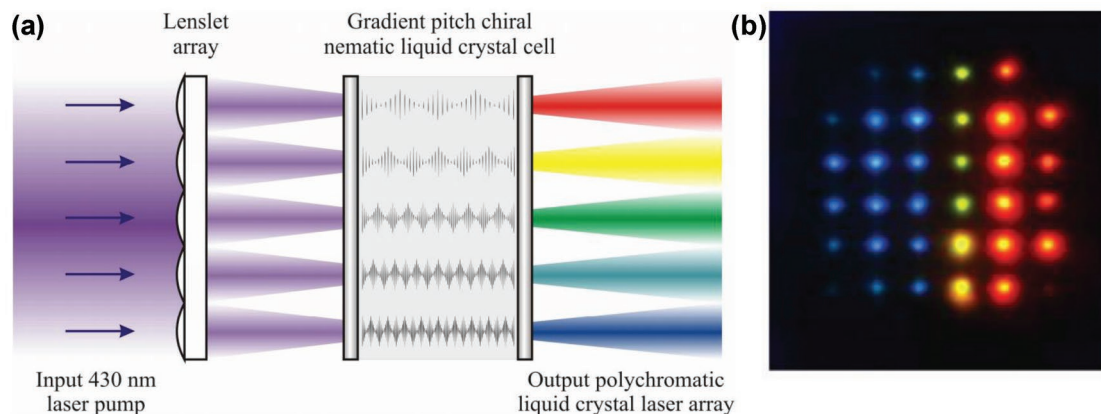


Figure 21. a) Illustration of a polychromatic CL laser array. b) Image of liquid crystal red–green–blue laser emission from a conventional LC cell when pumped by a microlens array. Reproduced with permission.^[73] Copyright 2008, Optical Society of America.

those of the semiconductor counterparts, which could be an excellent candidate for application to PICs.^[233] Alternatively, diode-pumped conjugated polymer lasers have become more compact, mechanically flexible, and offering a wide range wavelength tunability.^[145] Furthermore, soft-matter such as polymer materials can serve as both optical cavity and encapsulation for the realization of robust semiconductor colloid lasers that cover the whole visible spectrum.^[230]

In general, the applications of soft-matter microlasers are highly diverse ranging from tunable laser sources to biosensing and display applications. With regard to the wavelength tunability, soft-matter lasers offer better flexibility compared with their conventional semiconductor counterparts. For instance, the lasing wavelength of LC lasers can be readily tuned by mechanical deformation, temperature, and electric field.^[44] For sensing applications, the ability to produce lasers inside living cells and use them as intracellular probes is unique.^[45] Recently, intracellular plasmonic nanolasers,^[273] semiconductor nanowires,^[274] and nanodisks^[275] have also applied for detecting cellular environmental changes and cell-tagging. Likely, biocompatible and biodegradable materials are highly desired for these applications. With the development of novel, low-threshold, and efficient laser sources, it is expected that microlasers will be applied for in vitro and in vivo biomedical applications shortly.

It has been demonstrated that soft-matter microlasers are emerging research area. However, there are some challenges which have to be addressed in order to make them more appropriate for practical applications. For example, despite the unique properties, such as the biocompatibility and biodegradability, biomaterials used for photonic applications typically require complicated synthesis steps, which leads to relatively high cost.^[181] Another issue is that the emitting biomaterials generally suffer low quantum yield and photostability. Furthermore, microlasers based on living cells and bacteria are appealing but they require external cavities.^[177,178] Last but not least, most of the available biolasers possess size in a millimeter-scale (except the microsphere or droplet lasers) at this moment, which hinders their applications for implantation and biointegration.

Also, we believe that soft-matter microcavities and microlasers are expanding their applications beyond what we have

discussed above with the further advance of this field. Here we would like to present some potential examples. First, the polymer cavities can be promising for the studies of optical chaos^[276] and directional emission lasers.^[277] These studies rely on the deformed cavities such as elliptical structures that can be easily obtained from soft-matter spherical cavities by mechanical deformation.^[24] Very recently, Zhang et al. have demonstrated directional laser emission from a deformed limaçon microdisk.^[99] Using DLW or solution-printing technique, laser cavities with special configurations might be directly produced for the realization of directional emission. Second, the study of strong coupling between exciton and photon is also an interesting topic. In 1998, Lidzey et al. reported the first observation of the strong coupling regime based on a semiconductor polymer, opening a possibility to realize soft-matter polariton lasing.^[278] Very recently, Dietrich et al. demonstrated that exciton–polariton laser based on protein materials is practical and a critical step toward continuous-wave polariton lasing at room temperature.^[190] Third, the integration of soft-matter with low-toxic semiconductor colloids^[279] resulting in hybrid microlasers would be more attractive for biological sensing. In these hybrid lasers, the photostability of conventional dye-doped soft-matter lasers, specifically biolasers, is largely enhanced while retaining their inherent properties such as biocompatibility. Fourth, incorporating responsive dyes into microlasers for in vivo continuous analyte monitoring would be highly useful for biomedical applications.^[280] Last but not least, soft-matter microlasers made of disordered media would be an exciting topic to investigate. So far, this kind of tiny random lasers was primarily obtained using semiconductor materials rather than soft-matter.^[281,282] It is expected that such micrometer-sized random lasers may be much more cost-effective compared with conventional microlasers.

Acknowledgements

This research is funded by Vietnam National Foundation for Science and Technology Development (NAFOSTED) under grant number 103.03-2017.318 and the Singapore Ministry of Education through the Academic Research Fund under Projects MOE2016-T2-1-054, Tier 1-RG105/16, and Tier 1- RG92/15.

Conflict of Interest

The authors declare no conflict of interest.

Keywords

biolasers, microlasers, polymer lasers, self-assembly, soft-matter photonics

Received: January 9, 2019

Revised: March 1, 2019

Published online:

- [1] K. J. Vahala, *Nature* **2003**, 424, 839.
- [2] Y. Yamamoto, R. E. Slusher, *Phys. Today* **1993**, 46, 66.
- [3] J. Kasprzak, M. Richard, S. Kundermann, A. Baas, P. Jeambrun, J. M. J. Keeling, F. M. Marchetti, M. H. Szymariska, R. André, J. L. Staehli, V. Savona, P. B. Littlewood, B. Deveaud, L. S. Dang, *Nature* **2006**, 443, 409.
- [4] S. Kéna-Cohen, S. R. Forrest, *Nat. Photonics* **2010**, 4, 371.
- [5] M. T. Hill, M. C. Gather, *Nat. Photonics* **2014**, 8, 908.
- [6] D. S. Wiersma, *Nat. Phys.* **2008**, 4, 359.
- [7] T. H. Maiman, *Nature* **1960**, 187, 493.
- [8] Y. H. Lee, J. L. Jewell, A. Scherer, S. L. McCall, J. P. Harbison, L. T. Florez, *Electron. Lett.* **1989**, 25, 1377.
- [9] S. L. McCall, A. F. J. Levi, R. E. Slusher, S. J. Pearton, R. A. Logan, *Appl. Phys. Lett.* **1992**, 60, 289.
- [10] M. Cai, O. Painter, K. J. Vahala, P. C. Sercel, *Opt. Lett.* **2000**, 25, 1430.
- [11] S. M. Spillane, T. J. Kippenberg, K. J. Vahala, *Nature* **2002**, 415, 621.
- [12] O. Painter, R. K. Lee, A. Scherer, A. Yariv, J. D. O'Brien, P. D. Dapkus, I. Kim, *Science* **1999**, 284, 1819.
- [13] M. H. Huang, S. Mao, H. Feick, H. Yan, Y. Wu, H. Kind, E. Weber, R. Russo, P. Yang, *Science* **2001**, 292, 1897.
- [14] V. I. Klimov, A. A. Mikhailovsky, S. Xu, A. Malko, J. A. Hollingsworth, C. A. Leatherdale, H.-J. Eisler, M. G. Bawendi, *Science* **2000**, 290, 314.
- [15] C. Dang, J. Lee, C. Breen, J. S. Steckel, S. Coe-Sullivan, A. Nurmikko, *Nat. Nanotechnol.* **2012**, 7, 335.
- [16] Y. Wang, K. S. Leck, V. D. Ta, R. Chen, V. Nalla, Y. Gao, T. He, H. V. Demir, H. Sun, *Adv. Mater.* **2015**, 27, 169.
- [17] G. Xing, N. Mathews, S. S. Lim, N. Yantara, X. Liu, D. Sabba, M. Grätzel, S. Mhaisalkar, T. C. Sum, *Nat. Mater.* **2014**, 13, 476.
- [18] S. W. Eaton, M. Lai, N. A. Gibson, A. B. Wong, L. Dou, J. Ma, L.-W. Wang, S. R. Leone, P. Yang, *Proc. Natl. Acad. Sci. USA* **2016**, 113, 1993.
- [19] Y. Wang, X. Li, V. Nalla, H. Zeng, H. Sun, *Adv. Funct. Mater.* **2017**, 27, 1605088.
- [20] Y. Jia, R. A. Kerner, A. J. Grede, B. P. Rand, N. C. Giebink, *Nat. Photonics* **2017**, 11, 784.
- [21] Y. Wang, H. Sun, *Small Methods* **2018**, 2, 1700252.
- [22] I. D. W. Samuel, G. A. Turnbull, *Chem. Rev.* **2007**, 107, 1272.
- [23] J. Clark, G. Lanzani, *Nat. Photonics* **2010**, 4, 438.
- [24] V. D. Ta, R. Chen, H. D. Sun, *Sci. Rep.* **2013**, 3, 1362.
- [25] I. D. W. Samuel, G. A. Turnbull, *Mater. Today* **2004**, 7, 28.
- [26] C. Grivas, M. Pollnau, *Laser Photonics Rev.* **2012**, 6, 419.
- [27] S. Chénais, S. Forget, *Polym. Int.* **2012**, 61, 390.
- [28] J. Herrnsdorf, Y. Wang, J. J. D. McKendry, Z. Gong, D. Massoubre, B. Guilhabert, G. Tsiminis, G. A. Turnbull, I. D. W. Samuel, N. Laurand, E. Gu, M. D. Dawson, *Laser Photonics Rev.* **2013**, 7, 1065.
- [29] W. Zhang, J. Yao, Y. S. Zhao, *Acc. Chem. Res.* **2016**, 49, 1691.
- [30] A. J. C. Kuehne, M. C. Gather, *Chem. Rev.* **2016**, 116, 12823.
- [31] C. Monat, P. Domachuk, B. J. Eggleton, *Nat. Photonics* **2007**, 1, 106.
- [32] H. Schmidt, A. R. Hawkins, *Nat. Photonics* **2011**, 5, 598.
- [33] X. Fan, S.-H. Yun, *Nat. Methods* **2014**, 11, 141.
- [34] M. Aas, A. Jonáš, A. Kiraz, *Opt. Commun.* **2013**, 290, 183.
- [35] Y. Wang, H. Li, L. Zhao, B. Wu, S. Liu, Y. Liu, J. Yang, *Opt. Laser Technol.* **2016**, 86, 61.
- [36] D. McGloin, *Rep. Prog. Phys.* **2017**, 80, 054402.
- [37] J. Ward, O. Benson, *Laser Photonics Rev.* **2011**, 5, 553.
- [38] L. He, Ş. K. Özdemir, L. Yang, *Laser Photonics Rev.* **2012**, 7, 1.
- [39] S. Yang, Y. Wang, H. Sun, *Adv. Opt. Mater.* **2015**, 3, 1136.
- [40] X.-F. Jiang, C.-L. Zou, L. Wang, Q. Gong, Y.-F. Xiao, *Laser Photonics Rev.* **2016**, 10, 40.
- [41] T. Reynolds, N. Riesen, A. Meldrum, X. Fan, J. M. M. Hall, T. M. Monro, A. François, *Laser Photonics Rev.* **2017**, 11, 1600265.
- [42] HumarM, RavnikM, PajkS, MusevicI, *Nat. Photonics* **2009**, 3, 595.
- [43] I. D. W. Samuel, *Nature* **2004**, 429, 709.
- [44] H. Coles, S. Morris, *Nat. Photonics* **2010**, 4, 676.
- [45] M. Humar, S. Hyun Yun, *Nat. Photonics* **2015**, 9, 572.
- [46] M. Schubert, A. Steude, P. Liehm, N. M. Kronenberg, M. Karl, E. C. Campbell, S. J. Powis, M. C. Gather, *Nano Lett.* **2015**, 15, 5647.
- [47] C. G. B. Garrett, W. Kaiser, W. L. Bond, *Phys. Rev.* **1961**, 124, 1807.
- [48] L. Rayleigh, *London, Edinburgh, Dublin Philos. Mag. J. Sci.* **1910**, 20, 1001.
- [49] R. Benner, P. Barber, J. Owen, R. Chang, *Phys. Rev. Lett.* **1980**, 44, 475.
- [50] H. M. Tzeng, K. F. Wall, M. B. Long, R. K. Chang, *Opt. Lett.* **1984**, 9, 499.
- [51] H. B. Lin, A. L. Huston, B. L. Justus, A. J. Campillo, *Opt. Lett.* **1986**, 11, 614.
- [52] S. X. Qian, J. B. Snow, H. M. Tzeng, R. K. Chang, *Science* **1986**, 231, 486.
- [53] C. C. Lam, P. T. Leung, K. Young, *J. Opt. Soc. Am. B* **1992**, 9, 1585.
- [54] J. Haase, S. Shinohara, P. Mundra, G. Risse, V. G. Lyssenko, H. Fröb, M. Hentschel, A. Eychmüller, K. Leo, *Appl. Phys. Lett.* **2010**, 97, 211101.
- [55] A. Ashkin, J. M. Dziedzic, *Science* **1975**, 187, 1073.
- [56] J. Schäfer, J. P. Mondia, R. Sharma, Z. H. Lu, A. S. Susha, A. L. Rogach, L. J. Wang, *Nano Lett.* **2008**, 8, 1709.
- [57] M. Ma, R. M. Hill, *Curr. Opin. Colloid Interface Sci.* **2006**, 11, 193.
- [58] E. Hosono, S. Fujihara, I. Honma, H. Zhou, *J. Am. Chem. Soc.* **2005**, 127, 13458.
- [59] V. D. Ta, A. Dunn, T. J. Wasley, J. Li, R. W. Kay, J. Stringer, P. J. Smith, E. Esenturk, C. Connaughton, J. D. Shephard, *Appl. Surf. Sci.* **2016**, 365, 153.
- [60] A. Kiraz, A. Sennaroglu, S. Doğanay, M. A. Dündar, A. Kurt, H. Kalaycıoğlu, A. L. Demirel, *Opt. Commun.* **2007**, 276, 145.
- [61] A. Sennaroglu, A. Kiraz, M. A. Dündar, A. Kurt, A. L. Demirel, *Opt. Lett.* **2007**, 32, 2197.
- [62] R. Sharma, J. P. Mondia, J. Schäfer, Z. H. Lu, L. J. Wang, *J. Appl. Phys.* **2009**, 105, 113104.
- [63] A. Kiraz, Y. Karadağ, A. F. Coskun, *Appl. Phys. Lett.* **2008**, 92, 191104.
- [64] S. Nizamoglu, M. C. Gather, S. H. Yun, *Adv. Mater.* **2013**, 25, 5943.
- [65] A. J. R. Lasprilla, G. A. R. Martinez, B. H. Lunelli, A. L. Jardini, R. M. Filho, *Biotechnol. Adv.* **2012**, 30, 321.
- [66] A. Jonas, M. Aas, Y. Karadağ, S. Manioglou, S. Anand, D. McGloin, H. Bayraktar, A. Kiraz, *Lab Chip* **2014**, 14, 3093.
- [67] S. Yang, V. D. Ta, Y. Wang, R. Chen, T. He, H. V. Demir, H. Sun, *Sci. Rep.* **2016**, 6, 27200.
- [68] *Liquid Crystals Beyond Displays: Chemistry, Physics, and Applications* (Ed: Q. Li), John Wiley & Sons, Hoboken, NJ **2012**.
- [69] M. Humar, *Liq. Cryst.* **2016**, 43, 1937.

- [70] P. V. Shibaev, B. Crooker, M. Manevich, E. Hanelt, *Appl. Phys. Lett.* **2011**, *99*, 233302.
- [71] Y. Wang, H. Li, L. Zhao, Y. Liu, S. Liu, J. Yang, *Appl. Phys. Lett.* **2016**, *109*, 231906.
- [72] G. Petriashvili, M. De Santo, R. Barberi, R. J. Hernandez, G. Cipparrone, *Soft Matter* **2017**, *13*, 6227.
- [73] S. M. Morris, P. J. W. Hands, S. Findeisen-Tandel, R. H. Cole, T. D. Wilkinson, H. J. Coles, *Opt. Express* **2008**, *16*, 18827.
- [74] M. Humar, I. Mušević, *Opt. Express* **2011**, *19*, 19836.
- [75] M. Humar, I. Musevic, *Opt. Express* **2010**, *18*, 26995.
- [76] M. Tanyeri, R. Perron, I. M. Kennedy, *Opt. Lett.* **2007**, *32*, 2529.
- [77] A. J. C. Kuehne, M. C. Gather, I. A. Eydelnant, S.-H. Yun, D. A. Weitz, A. R. Wheeler, *Lab Chip* **2011**, *11*, 3716.
- [78] S. K. Y. Tang, Z. Li, A. R. Abate, J. J. Agresti, D. A. Weitz, D. Psaltis, G. M. Whitesides, *Lab Chip* **2009**, *9*, 2767.
- [79] L.-J. Chen, L.-L. Gong, Y.-L. Lin, X.-Y. Jin, H.-Y. Li, S.-S. Li, K.-J. Che, Z.-P. Cai, C. J. Yang, *Lab Chip* **2016**, *16*, 1206.
- [80] G. Aubry, Q. Kou, J. Soto-Velasco, C. Wang, S. Meance, J. J. He, A. M. Haghiri-Gosnet, *Appl. Phys. Lett.* **2011**, *98*, 111111.
- [81] D. L. Chen, R. F. Ismagilov, *Curr. Opin. Chem. Biol.* **2006**, *10*, 226.
- [82] M. Saito, H. Shimatani, H. Naruhashi, *Opt. Express* **2008**, *16*, 11915.
- [83] M. Schubert, K. Volckaert, M. Karl, A. Morton, P. Liehm, G. B. Miles, S. J. Powis, M. C. Gather, *Sci. Rep.* **2017**, *7*, 40877.
- [84] K.-G. Makoto, T. Kenji, Y. Hiroaki, E. Kazuhiro, *Jpn. J. Appl. Phys.* **1992**, *31*, L99.
- [85] M. Kuwata-Gonokami, K. Takeda, *Opt. Mater.* **1998**, *9*, 12.
- [86] V. D. Ta, R. Chen, H. D. Sun, *Adv. Mater.* **2012**, *24*, OP60.
- [87] M. Kuwata-Gonokami, R. H. Jordan, A. Dodabalapur, H. E. Katz, M. L. Schilling, R. E. Slusher, S. Ozawa, *Opt. Lett.* **1995**, *20*, 2093.
- [88] A. Camposeo, F. Di Benedetto, R. Stabile, A. A. R. Neves, R. Cingolani, D. Pisignano, *Small* **2009**, *5*, 562.
- [89] T. Grossmann, S. Schleede, M. Hauser, M. B. Christiansen, C. Vannahme, C. Eschenbaum, S. Klinkhammer, T. Beck, J. Fuchs, G. U. Nienhaus, U. Lemmer, A. Kristensen, T. Mappes, H. Kalt, *Appl. Phys. Lett.* **2010**, *97*, 063304.
- [90] M. D. McGehee, M. A. D'áz-García, F. Hide, R. Gupta, E. K. Miller, D. Moses, A. J. Heeger, *Appl. Phys. Lett.* **1998**, *72*, 1536.
- [91] T. Zhai, F. Cao, S. Chu, Q. Gong, X. Zhang, *Opt. Express* **2018**, *26*, 4491.
- [92] M. Karl, J. M. E. Glackin, M. Schubert, N. M. Kronenberg, G. A. Turnbull, I. D. W. Samuel, M. C. Gather, *Nat. Commun.* **2018**, *9*, 1525.
- [93] S. Schauer, X. Liu, M. Worgull, U. Lemmer, H. Hölscher, *Opt. Mater. Express* **2015**, *5*, 576.
- [94] T. Zhai, X. Zhang, Z. Pang, *Opt. Express* **2011**, *19*, 6487.
- [95] C. Vannahme, C. L. C. Smith, M. B. Christiansen, A. Kristensen, *Appl. Phys. Lett.* **2012**, *101*, 151123.
- [96] T. Zhai, Y. Wang, L. Chen, X. Wu, S. Li, X. Zhang, *Nanoscale* **2015**, *7*, 19935.
- [97] Z. Li, D. Psaltis, *IEEE J. Sel. Top. Quantum Electron.* **2007**, *13*, 185.
- [98] T. Grossmann, S. Schleede, M. Hauser, T. Beck, M. Thiel, G. von Freymann, T. Mappes, H. Kalt, *Opt. Express* **2011**, *19*, 11451.
- [99] N. Zhang, Y. Wang, W. Sun, S. Liu, C. Huang, X. Jiang, M. Xiao, S. Xiao, Q. Song, *Nanoscale* **2018**, *10*, 2045.
- [100] H. Hodaei, M.-A. Miri, M. Heinrich, D. N. Christodoulides, M. Khajavikhan, *Science* **2014**, *346*, 975.
- [101] L. Chang, X. Jiang, S. Hua, C. Yang, J. Wen, L. Jiang, G. Li, G. Wang, M. Xiao, *Nat. Photonics* **2014**, *8*, 524.
- [102] B. Peng, S. K. Ozdemir, F. Lei, F. Monifi, M. Gianfreda, G. L. Long, S. Fan, F. Nori, C. M. Bender, L. Yang, *Nat. Phys.* **2014**, *10*, 394.
- [103] Z. Gu, N. Zhang, Q. Lyu, M. Li, S. Xiao, Q. Song, *Laser Photonics Rev.* **2016**, *10*, 588.
- [104] V. S. Ilchenko, A. B. Matsko, *IEEE J. Sel. Top. Quantum Electron.* **2006**, *12*, 15.
- [105] V. D. Ta, S. Yang, Y. Wang, Y. Gao, T. He, R. Chen, H. V. Demir, H. Sun, *Appl. Phys. Lett.* **2015**, *107*, 221103.
- [106] R. Chen, V. D. Ta, H. D. Sun, *Sci. Rep.* **2012**, *2*, 244.
- [107] V. D. Ta, R. Chen, D. M. Nguyen, H. D. Sun, *Appl. Phys. Lett.* **2013**, *102*, 031107.
- [108] Y. Wang, S. Yang, H. Yang, H. Sun, *Adv. Opt. Mater.* **2015**, *3*, 652.
- [109] R. Chen, V. D. Ta, F. Xiao, Q. Zhang, H. Sun, *Small* **2013**, *9*, 1052.
- [110] A. Camposeo, L. Persano, D. Pisignano, *Macromol. Mater. Eng.* **2013**, *298*, 487.
- [111] A. Garreau, J.-L. Duvail, *Adv. Opt. Mater.* **2014**, *2*, 1122.
- [112] L. Persano, A. Camposeo, D. Pisignano, *Prog. Polym. Sci.* **2015**, *43*, 48.
- [113] A. J. Das, C. Lafargue, M. Lebental, J. Zyss, K. S. Narayan, *Appl. Phys. Lett.* **2011**, *99*, 263303.
- [114] L. Persano, A. Camposeo, P. D. Carro, V. Fasano, M. Moffa, R. Manco, S. D'Agostino, D. Pisignano, *Adv. Mater.* **2014**, *26*, 6542.
- [115] V. D. Ta, R. Chen, H. Sun, *Adv. Opt. Mater.* **2014**, *2*, 220.
- [116] V. D. Ta, R. Chen, L. Ma, Y. J. Ying, H. D. Sun, *Laser Photonics Rev.* **2013**, *7*, 133.
- [117] X. Yang, B. Li, *ACS Macro Lett.* **2014**, *3*, 1266.
- [118] H. Li, J. Li, L. Qiang, Y. Zhang, S. Hao, *Nanoscale* **2013**, *5*, 6297.
- [119] S. Qinghai, L. Liu, L. Xu, *J. Lightwave Technol.* **2009**, *27*, 4374.
- [120] S. Huijin, Z. Hua, F. Guoying, Z. Hao, Z. Shouhuan, *Laser Phys. Lett.* **2017**, *14*, 055806.
- [121] S. Krämmer, F. Laye, F. Friedrich, C. Vannahme, C. L. C. Smith, A. C. Mendes, I. S. Chronakis, J. Lahann, A. Kristensen, H. Kalt, *Adv. Opt. Mater.* **2017**, *5*, 1700248.
- [122] F. Guo, H. You, D. Zhang, S. Chen, *Org. Electron.* **2018**, *63*, 52.
- [123] S. Kim, S. Yang, S. H. Choi, Y. L. Kim, W. Ryu, C. Joo, *Sci. Rep.* **2017**, *7*, 4506.
- [124] S. Krämmer, C. Vannahme, C. L. C. Smith, T. Grossmann, M. Jenne, S. Schierle, L. Jørgensen, I. S. Chronakis, A. Kristensen, H. Kalt, *Adv. Mater.* **2014**, *26*, 8096.
- [125] S. Li, L. Wang, T. Zhai, L. Chen, M. Wang, Y. Wang, F. Tong, Y. Wang, X. Zhang, *Opt. Express* **2016**, *24*, 12748.
- [126] R. Zhang, S. Knitter, S. F. Liew, F. G. Omenetto, B. M. Reinhard, H. Cao, L. D. Negro, *Appl. Phys. Lett.* **2016**, *108*, 011103.
- [127] M. C. Albuquerque de Oliveira, L. de Souza Menezes, P. I. R. Pincheira, C. Rojas-Ulloa, N. R. Gomez, H. P. de Oliveira, A. S. Leônidas Gomes, *Nanoscale Adv.* **2019**, *1*, 728.
- [128] K. Oda, N. Takato, H. Toba, *J. Lightwave Technol.* **1991**, *9*, 728.
- [129] X. Jiang, Y. Chen, G. Vienne, L. Tong, *Opt. Lett.* **2007**, *32*, 1710.
- [130] U. Scherf, S. Riechel, U. Lemmer, R. F. Mahrt, *Curr. Opin. Solid State Mater. Sci.* **2001**, *5*, 143.
- [131] D. Moses, *Appl. Phys. Lett.* **1992**, *60*, 3215.
- [132] N. Tessler, G. J. Denton, R. H. Friend, *Nature* **1996**, *382*, 695.
- [133] S. V. Frolov, M. Shkunov, Z. V. Vardeny, K. Yoshino, *Phys. Rev. B* **1997**, *56*, R4363.
- [134] G. Heliotis, R. Xia, G. A. Turnbull, P. Andrew, W. L. Barnes, I. D. W. Samuel, D. D. C. Bradley, *Adv. Funct. Mater.* **2004**, *14*, 91.
- [135] G. Heliotis, R. Xia, D. D. C. Bradley, G. A. Turnbull, I. D. W. Samuel, P. Andrew, W. L. Barnes, *J. Appl. Phys.* **2004**, *96*, 6959.
- [136] M. Reufer, S. Riechel, J. M. Lupton, J. Feldmann, U. Lemmer, D. Schneider, T. Benstem, T. Dobbertin, W. Kowalsky, A. Gombert, K. Forberich, V. Wittwer, U. Scherf, *Appl. Phys. Lett.* **2004**, *84*, 3262.
- [137] C. Karnutsch, C. Pflumm, G. Heliotis, J. C. deMello, D. D. C. Bradley, J. Wang, T. Weimann, V. Haug, C. Gärtner, U. Lemmer, *Appl. Phys. Lett.* **2007**, *90*, 131104.
- [138] S. Li, W.-F. Jiang, Y.-P. Xu, T. F. George, *J. Phys. Chem. C* **2011**, *115*, 17582.
- [139] D. O'Carroll, I. Lieberwirth, G. Redmond, *Nat. Nanotechnol.* **2007**, *2*, 180.

- [140] S. Kushida, D. Okada, F. Sasaki, Z.-H. Lin, J.-S. Huang, Y. Yamamoto, *Adv. Opt. Mater.* **2017**, *5*, 1700123.
- [141] D. M. Coles, A. A. P. Trichet, P. R. Dolan, R. A. Taylor, C. Vallance, J. M. Smith, *Laser Photonics Rev.* **2015**, *9*, 538.
- [142] A. Tulek, D. Akbulut, M. Bayindir, *Appl. Phys. Lett.* **2009**, *94*, 203302.
- [143] Y. Yang, G. A. Turnbull, I. D. W. Samuel, *Appl. Phys. Lett.* **2008**, *92*, 163306.
- [144] G. Tsiminis, Y. Wang, A. L. Kanibolotsky, A. R. Inigo, P. J. Skabara, I. D. W. Samuel, G. A. Turnbull, *Adv. Mater.* **2013**, *25*, 2826.
- [145] C. Foucher, B. Guilhabert, J. Herrnsdorf, N. Laurand, M. D. Dawson, *Opt. Express* **2014**, *22*, 24160.
- [146] A. S. D. Sandanayaka, T. Matsushima, F. Bencheikh, K. Yoshida, M. Inoue, T. Fujihara, K. Goushi, J.-C. Ribierre, C. Adachi, *Sci. Adv.* **2017**, *3*, e1602570.
- [147] T. Hansch, M. Pernier, A. Schawlow, *IEEE J. Quantum Electron.* **1971**, *7*, 45.
- [148] H. Kogelnik, C. V. Shank, *Appl. Phys. Lett.* **1971**, *18*, 152.
- [149] X. Zhang, W. Lee, X. Fan, *Lab Chip* **2012**, *12*, 3673.
- [150] Y. Sun, X. Fan, *Angew. Chem., Int. Ed.* **2012**, *51*, 1236.
- [151] Q. Chen, X. Zhang, Y. Sun, M. Ritt, S. Sivaramakrishnan, X. Fan, *Lab Chip* **2013**, *13*, 2679.
- [152] X. Wu, M. K. K. Oo, K. Reddy, Q. Chen, Y. Sun, X. Fan, *Nat. Commun.* **2014**, *5*, 3779.
- [153] Y.-C. Chen, Q. Chen, X. Fan, *Optica* **2016**, *3*, 809.
- [154] V. D. Ta, S. Caixeiro, F. M. Fernandes, R. Sapienza, *Adv. Opt. Mater.* **2017**, *5*, 1601022.
- [155] Y.-L. Sun, Z.-S. Hou, S.-M. Sun, B.-Y. Zheng, J.-F. Ku, W.-F. Dong, Q.-D. Chen, H.-B. Sun, *Sci. Rep.* **2015**, *5*, 12852.
- [156] Y. Wei, X. Lin, C. Wei, W. Zhang, Y. Yan, Y. S. Zhao, *ACS Nano* **2017**, *11*, 597.
- [157] L. Sznitko, P. Hanczyc, J. Mysliwiec, M. Samoc, *Appl. Phys. Lett.* **2015**, *106*, 023702.
- [158] M. Humar, A. Dobravec, X. Zhao, S. H. Yun, *Optica* **2017**, *4*, 1080.
- [159] S. Toffanin, S. Kim, S. Cavallini, M. Natali, V. Benfenati, J. J. Amsden, D. L. Kaplan, R. Zamboni, M. Muccini, F. G. Omenetto, *Appl. Phys. Lett.* **2012**, *101*, 091110.
- [160] Y. Choi, H. Jeon, S. Kim, *Lab Chip* **2015**, *15*, 642.
- [161] C. Vannahme, F. Maier-Flaig, U. Lemmer, A. Kristensen, *Lab Chip* **2013**, *13*, 2675.
- [162] D. S. Wiersma, *Nat. Photonics* **2013**, *7*, 188.
- [163] H. E. Türeci, L. Ge, S. Rotter, A. D. Stone, *Science* **2008**, *320*, 643.
- [164] H. Cao, Y. G. Zhao, S. T. Ho, E. W. Seelig, Q. H. Wang, R. P. H. Chang, *Phys. Rev. Lett.* **1999**, *82*, 2278.
- [165] Q. Song, L. Liu, S. Xiao, X. Zhou, W. Wang, L. Xu, *Phys. Rev. Lett.* **2006**, *96*, 033902.
- [166] B. Redding, M. A. Choma, H. Cao, *Nat. Photonics* **2012**, *6*, 355.
- [167] B. Redding, A. Cerjan, X. Huang, M. L. Lee, A. D. Stone, M. A. Choma, H. Cao, *Proc. Natl. Acad. Sci. USA* **2015**, *112*, 1304.
- [168] F. Lahoz, I. R. Martín, M. Urgellés, J. Marrero-Alonso, R. Marín, C. J. Saavedra, A. Boto, M. Díaz, *Laser Phys. Lett.* **2015**, *12*, 045805.
- [169] R. C. Polson, Z. V. Vardeny, *Appl. Phys. Lett.* **2004**, *85*, 1289.
- [170] Q. Song, S. Xiao, Z. Xu, J. Liu, X. Sun, V. Drachev, V. M. Shalaev, O. Akkus, Y. L. Kim, *Opt. Lett.* **2010**, *35*, 1425.
- [171] M. V. dos Santos, C. T. Dominguez, J. V. Schiavon, H. S. Barud, L. S. A. de Melo, S. J. L. Ribeiro, A. S. L. Gomes, C. B. de Araújo, *J. Appl. Phys.* **2014**, *115*, 083108.
- [172] I. Viola, N. Ghofraniha, A. Zacheo, V. Arima, C. Conti, G. Gigli, *J. Mater. Chem. C* **2013**, *1*, 8128.
- [173] S. Caixeiro, M. Gaio, B. Marelli, F. G. Omenetto, R. Sapienza, *Adv. Opt. Mater.* **2016**, *4*, 998.
- [174] W.-J. Lin, Y.-M. Liao, H.-Y. Lin, G. Haider, S.-Y. Lin, W.-C. Liao, R.-T. Wei, P. Perumal, T.-Y. Chang, C.-Y. Tseng, Y.-S. Lo, H.-M. Lin, T.-W. Shih, J.-S. Hwang, T.-Y. Lin, Y.-F. Chen, *Org. Electron.* **2018**, *62*, 209.
- [175] C.-S. Wang, T.-Y. Chang, T.-Y. Lin, Y.-F. Chen, *Sci. Rep.* **2015**, *4*, 6736.
- [176] W. Z. Wan Ismail, G. Liu, K. Zhang, E. M. Goldys, J. M. Dawes, *Opt. Express* **2016**, *24*, A85.
- [177] M. C. Gather, S. H. Yun, *Nat. Photonics* **2011**, *5*, 406.
- [178] M. C. Gather, S. H. Yun, *Opt. Lett.* **2011**, *36*, 3299.
- [179] M. D. McGehee, A. J. Heeger, *Adv. Mater.* **2000**, *12*, 1655.
- [180] M. Humar, S. S. J. Kwok, M. Choi, A. K. Yetisen, S. Cho, S. H. Yun, *Nanophotonics* **2016**, *5*, 60.
- [181] M. Jaroslaw, C. Konrad, S. Lech, M. Andrzej, *J. Optics* **2017**, *19*, 033003.
- [182] J. C. Hindman, R. Kugel, A. Svirnickas, J. J. Katz, *Proc. Natl. Acad. Sci. USA* **1977**, *74*, 5.
- [183] Y.-C. Chen, Q. Chen, X. Fan, *Lab Chip* **2016**, *16*, 2228.
- [184] X. Wu, Q. Chen, Y. Sun, X. Fan, *Appl. Phys. Lett.* **2013**, *102*, 203706.
- [185] S. J. Remington, *Protein Sci.* **2011**, *20*, 1509.
- [186] D. J. Pikas, S. M. Kirkpatrick, E. Tewksbury, L. L. Brott, R. R. Naik, M. O. Stone, W. M. Dennis, *J. Phys. Chem. B* **2002**, *106*, 4831.
- [187] M. C. Gather, S. H. Yun, *Nat. Commun.* **2014**, *5*, 5722.
- [188] C. P. Dietrich, S. Höfling, M. C. Gather, *Appl. Phys. Lett.* **2014**, *105*, 233702.
- [189] H. J. Oh, M. C. Gather, J.-J. Song, S. H. Yun, *Opt. Express* **2014**, *22*, 31411.
- [190] C. P. Dietrich, A. Steude, L. Töpf, M. Schubert, N. M. Kronenberg, K. Ostermann, S. Höfling, M. C. Gather, *Sci. Adv.* **2016**, *2*, e1600666.
- [191] M. Kuwata-Gonokami, presented at *Proc. LEOS '93*, San Jose, CA, USA November **1993**.
- [192] A. François, N. Riesen, H. Ji, S. A. V., T. M. Monro, *Appl. Phys. Lett.* **2015**, *106*, 031104.
- [193] H. Ridley, *Brit. J. Ophthalmol.* **1952**, *36*, 113.
- [194] J. M. Cariou, J. Dugas, L. Martin, P. Michel, *Appl. Opt.* **1986**, *25*, 334.
- [195] T. Wienhold, S. Kraemmer, S. F. Wondimu, T. Siegle, U. Bog, U. Weinzierl, S. Schmidt, H. Becker, H. Kalt, T. Mappes, S. Koeber, C. Koos, *Lab Chip* **2015**, *15*, 3800.
- [196] A. M. Flatae, M. Burrelli, H. Zeng, S. Nocentini, S. Wiegele, C. Parmeggiani, H. Kalt, D. Wiersma, *Light: Sci. Appl.* **2015**, *4*, e282.
- [197] L. Chen, Y. Li, J. Fan, H. K. Bisoyi, D. A. Weitz, Q. Li, *Adv. Opt. Mater.* **2014**, *2*, 845.
- [198] W. Y. Cao, A. Munoz, P. Palffy-Muhoray, B. Taheri, *Nat. Mater.* **2002**, *1*, 111.
- [199] J. Fan, Y. Li, H. K. Bisoyi, R. S. Zola, D.-k. Yang, T. J. Bunning, D. A. Weitz, Q. Li, *Angew. Chem., Int. Ed.* **2015**, *54*, 2160.
- [200] Z.-g. Zheng, R. S. Zola, H. K. Bisoyi, L. Wang, Y. Li, T. J. Bunning, Q. Li, *Adv. Mater.* **2017**, *29*, 1701903.
- [201] R. S. Zola, H. K. Bisoyi, H. Wang, A. M. Urbas, T. J. Bunning, Q. Li, *Adv. Mater.* **2019**, *31*, 1806172.
- [202] F. G. Omenetto, D. L. Kaplan, *Nat. Photonics* **2008**, *2*, 641.
- [203] F. G. Omenetto, D. L. Kaplan, *Science* **2010**, *329*, 528.
- [204] H. Tao, D. L. Kaplan, F. G. Omenetto, *Adv. Mater.* **2012**, *24*, 2824.
- [205] D. N. Rockwood, R. C. Preda, T. Yucel, X. Wang, M. L. Lovett, D. L. Kaplan, *Nat. Protoc.* **2011**, *6*, 1612.
- [206] S. Kim, A. N. Mitropoulos, J. D. Spitzberg, H. Tao, D. L. Kaplan, F. G. Omenetto, *Nat. Photonics* **2012**, *6*, 818.
- [207] S. T. Parker, P. Domachuk, J. Amsden, J. Bressner, J. A. Lewis, D. L. Kaplan, F. G. Omenetto, *Adv. Mater.* **2009**, *21*, 2411.
- [208] S. Kujala, A. Mannila, L. Karvonen, K. Kieu, Z. Sun, *Sci. Rep.* **2016**, *6*, 22358.
- [209] Y. Y. Diao, X. Y. Liu, G. W. Toh, L. Shi, J. Zi, *Adv. Funct. Mater.* **2013**, *23*, 5373.
- [210] L. Xu, X. Jiang, G. Zhao, D. Ma, H. Tao, Z. Liu, F. G. Omenetto, L. Yang, *Opt. Express* **2016**, *24*, 20825.

- [211] R. R. da Silva, C. T. Dominguez, M. V. dos Santos, R. Barbosa-Silva, M. Cavicchioli, L. M. Christovan, L. S. A. de Melo, A. S. L. Gomes, C. B. de Araújo, S. J. L. Ribeiro, *J. Mater. Chem. C* **2013**, 1, 7181.
- [212] I. B. Dogru, R. Melikov, S. Nizamoglu, *ACS Biomater. Sci. Eng.* **2018**, 4, 4385.
- [213] A. J. Steckl, *Nat. Photonics* **2007**, 1, 3.
- [214] Y. Kawabe, L. Wang, S. Horinouchi, N. Ogata, *Adv. Mater.* **2000**, 12, 1281.
- [215] Y. Kawabe, L. Wang, T. Nakamura, N. Ogata, *Appl. Phys. Lett.* **2002**, 81, 1372.
- [216] Z. Yu, W. Li, J. A. Hagen, Y. Zhou, D. Klotzkin, J. G. Grote, A. J. Steckl, *Appl. Opt.* **2007**, 46, 1507.
- [217] M. Leonetti, R. Sapienza, M. Ibsate, C. Conti, C. López, *Opt. Lett.* **2009**, 34, 3764.
- [218] I. Rau, A. Szukalski, L. Sznitko, A. Miniewicz, S. Bartkiewicz, F. Kajzar, B. Sahraoui, J. Mysliwiec, *Appl. Phys. Lett.* **2012**, 101, 171113.
- [219] J. Mysliwiec, L. Sznitko, A. Miniewicz, F. Kajzar, B. Sahraoui, *J. Phys. D: Appl. Phys.* **2009**, 42, 085101.
- [220] J. Mysliwiec, L. Sznitko, A. Sobolewska, S. Bartkiewicz, A. Miniewicz, *Appl. Phys. Lett.* **2010**, 96, 141106.
- [221] A. Camposo, P. Del Carro, L. Persano, K. Cyprich, A. Szukalski, L. Sznitko, J. Mysliwiec, D. Pisignano, *ACS Nano* **2014**, 8, 10893.
- [222] C. Z. Ning, *Phys. Status Solidi B* **2010**, 4, 774.
- [223] R. Chen, H. D. Sun, T. Wang, K. N. Hui, H. W. Choi, *Appl. Phys. Lett.* **2010**, 96, 241101.
- [224] A. C. Tamboli, E. D. Haberer, R. Sharma, K. H. Lee, S. Nakamura, E. L. Hu, *Nat. Photonics* **2007**, 1, 61.
- [225] R. Chen, B. Ling, X. W. Sun, H. D. Sun, *Adv. Mater.* **2011**, 23, 2199.
- [226] J. A. Rogers, Z. Bao, M. Meier, A. Dodabalapur, O. J. A. Schueller, G. M. Whitesides, *Synth. Met.* **2000**, 115, 5.
- [227] J. Alamán, R. Alicante, J. Peña, C. Sánchez-Somolinos, *Materials* **2016**, 9, 910.
- [228] M. Deubel, G. von Freymann, M. Wegener, S. Pereira, K. Busch, C. M. Soukoulis, *Nat. Mater.* **2004**, 3, 444.
- [229] Y. Yan, Y. S. Zhao, *Chem. Soc. Rev.* **2014**, 43, 4325.
- [230] Y. Wang, V. D. Ta, K. S. Leck, B. H. I. Tan, Z. Wang, T. He, C.-D. Ohl, H. V. Demir, H. Sun, *Nano Lett.* **2017**, 17, 2640.
- [231] C. Wei, S.-Y. Liu, C.-L. Zou, Y. Liu, J. Yao, Y. S. Zhao, *J. Am. Chem. Soc.* **2015**, 137, 62.
- [232] F. S. F. Brossard, V. Pecunia, A. J. Ramsay, J. P. Griffiths, M. Hugues, H. Sirringhaus, *Adv. Mater.* **2017**, 29, 1704425.
- [233] C. Zhang, C.-L. Zou, Y. Zhao, C.-H. Dong, C. Wei, H. Wang, Y. Liu, G.-C. Guo, J. Yao, Y. S. Zhao, *Sci. Adv.* **2015**, 1, e1500257.
- [234] M. Saito, K. Koyama, *Jpn. J. Appl. Phys.* **2010**, 49, 092501.
- [235] L. Xin, K. Sönke, S. Kai, M. Norman, V. Christoph, K. Johannes, M. Timo, W. Martin, L. Uli, *Appl. Phys. Express* **2012**, 5, 072101.
- [236] D. J. Gardiner, W. K. Hsiao, S. M. Morris, P. J. W. Hands, T. D. Wilkinson, I. M. Hutchings, H. J. Coles, *Soft Matter* **2012**, 8, 9977.
- [237] Y.-M. Liao, W.-C. Liao, S.-W. Chang, C.-F. Hou, C.-T. Tai, C.-Y. Su, Y.-T. Hsu, M.-H. Wu, R.-J. Chou, Y.-H. Lee, S.-Y. Lin, W.-J. Lin, C.-H. Chang, G. Haider, M. Kataria, P. K. Roy, K. P. Bera, C. R. Paulinbaraj, H.-W. Hu, T.-Y. Lin, Y.-F. Chen, *Adv. Mater. Technol.* **2018**, 3, 1800214.
- [238] Y. Wang, K. E. Fong, S. Yang, V. D. Ta, Y. Gao, Z. Wang, V. Nalla, H. V. Demir, H. Sun, *Laser Photonics Rev.* **2015**, 9, 507.
- [239] S. Kawata, H.-B. Sun, T. Tanaka, K. Takada, *Nature* **2001**, 412, 697.
- [240] S. Wong, M. Deubel, F. Pérez-Willard, S. John, G. A. Ozin, M. Wegener, G. von Freymann, *Adv. Mater.* **2006**, 18, 265.
- [241] T. Gissibl, S. Thiele, A. Herkommer, H. Giessen, *Nat. Photonics* **2016**, 10, 554.
- [242] Z.-P. Liu, Y. Li, Y.-F. Xiao, B.-B. Li, X.-F. Jiang, Y. Qin, X.-B. Feng, H. Yang, Q. Gong, *Appl. Phys. Lett.* **2010**, 97, 211105.
- [243] Y.-L. Sun, W.-F. Dong, L.-G. Niu, T. Jiang, D.-X. Liu, L. Zhang, Y.-S. Wang, Q.-D. Chen, D.-P. Kim, H.-B. Sun, *Light: Sci. Appl.* **2014**, 3, e129.
- [244] M. Lu, S. S. Choi, C. J. Wagner, J. G. Eden, B. T. Cunningham, *Appl. Phys. Lett.* **2008**, 92, 261502.
- [245] D. Li, Y. Xia, *Adv. Mater.* **2004**, 16, 1151.
- [246] S. Ramakrishna, K. Fujihara, W.-E. Teo, T. Yong, Z. Ma, R. Ramaseshan, *Mater. Today* **2006**, 9, 40.
- [247] J. Xue, J. Xie, W. Liu, Y. Xia, *Acc. Chem. Res.* **2017**, 50, 1976.
- [248] R.-M. Ma, X. Yin, R. F. Oulton, V. J. Sorger, X. Zhang, *Nano Lett.* **2012**, 12, 5396.
- [249] L. He, S. K. Özdemir, J. Zhu, W. Kim, L. Yang, *Nat. Nanotechnol.* **2011**, 6, 428.
- [250] D. J. Gardiner, S. M. Morris, P. J. W. Hands, C. Mowatt, R. Rutledge, T. D. Wilkinson, H. J. Coles, *Opt. Express* **2011**, 19, 2432.
- [251] S. K. Y. Tang, R. Derda, Q. Quan, M. Lončar, G. M. Whitesides, *Opt. Express* **2011**, 19, 2204.
- [252] G. Strangi, V. Barna, R. Caputo, A. De Luca, C. Versace, N. Scaramuzza, C. Umeton, R. Bartolino, G. N. Price, *Phys. Rev. Lett.* **2005**, 94, 063903.
- [253] R. Chen, V. D. Ta, H. D. Sun, *ACS Photonics* **2014**, 1, 11.
- [254] P. Görrn, M. Lehnhardt, W. Kowalsky, T. Riedl, S. Wagner, *Adv. Mater.* **2011**, 23, 869.
- [255] S. M. Wood, F. Castles, S. J. Elston, S. M. Morris, *RSC Adv.* **2016**, 6, 31919.
- [256] F. Vollmer, S. Arnold, *Nat. Methods* **2008**, 5, 591.
- [257] F. Vollmer, L. Yang, *Nanophotonics* **2012**, 1, 267.
- [258] E. Kim, M. D. Baaske, F. Vollmer, *Lab Chip* **2017**, 17, 1190.
- [259] S. Arnold, R. Ramjit, D. Keng, V. Kolchenko, I. Teraoka, *Faraday Discuss.* **2008**, 137, 65.
- [260] F. Vollmer, S. Arnold, D. Keng, *Proc. Natl. Acad. Sci. USA* **2008**, 105, 20701.
- [261] Z. Liu, L. Liu, Z. Zhu, Y. Zhang, Y. Wei, X. Zhang, E. Zhao, Y. Zhang, J. Yang, L. Yuan, *Opt. Lett.* **2016**, 41, 4649.
- [262] X. Xu, W. Chen, G. Zhao, Y. Li, C. Lu, L. Yang, *Light: Sci. Appl.* **2018**, 7, 62.
- [263] I.-H. Lin, D. S. Miller, P. J. Bertics, C. J. Murphy, J. J. de Pablo, N. L. Abbott, *Science* **2011**, 332, 1297.
- [264] M. Lu, S. S. Choi, U. Irfan, B. T. Cunningham, *Appl. Phys. Lett.* **2008**, 93, 111113.
- [265] P. J. W. Hands, S. M. Morris, T. D. Wilkinson, H. J. Coles, *Opt. Lett.* **2008**, 33, 515.
- [266] T. L. Koch, U. Koren, *IEEE J. Quantum Electron.* **1991**, 27, 641.
- [267] W. Bogaerts, D. Taillaert, B. Luyssaert, P. Dumon, J. V. Campenhout, P. Bienstman, D. V. Thourhout, R. Baets, V. Wiaux, S. Beckx, *Opt. Express* **2004**, 12, 1583.
- [268] A. Liu, L. Liao, Y. Chetrit, J. Basak, H. Nguyen, D. Rubin, M. Paniccia, *IEEE J. Sel. Top. Quantum Electron.* **2010**, 16, 23.
- [269] D. Dai, J. Bauters, J. E. Bowers, *Light: Sci. Appl.* **2012**, 1, e1.
- [270] A. Rahim, E. Ryckeboer, A. Z. Subramanian, S. Clemmen, B. Kuyken, A. Dhakal, A. Raza, A. Hermans, M. Muneeb, S. Dhoore, Y. Li, U. Dave, P. Bienstman, N. Le Thomas, G. Roelkens, D. Van Thourhout, P. Helin, S. Severi, X. Rottenberg, R. Baets, *J. Lightwave Technol.* **2017**, 35, 639.
- [271] L. Eldada, L. W. Shacklette, *IEEE J. Sel. Top. Quantum Electron.* **2000**, 6, 54.
- [272] A. V. Shneidman, K. P. Becker, M. A. Lukas, N. Torgerson, C. Wang, O. Reshef, M. J. Burek, K. Paul, J. McLellan, M. Lončar, *ACS Photonics* **2018**, 5, 1839.
- [273] E. I. Galanzha, R. Weingold, D. A. Nedosekin, M. Sarimollaoglu, J. Nolan, W. Harrington, A. S. Kuchyanov, R. G. Parkhomenko,

- F. Watanabe, Z. Nima, A. S. Biris, A. I. Plekhanov, M. I. Stockman, V. P. Zharov, *Nat. Commun.* **2017**, *8*, 15528.
- [274] X. Wu, Q. Chen, P. Xu, Y.-C. Chen, B. Wu, R. M. Coleman, L. Tong, X. Fan, *Nanoscale* **2018**, *10*, 9729.
- [275] A. H. Fikouras, M. Schubert, M. Karl, J. D. Kumar, S. J. Powis, A. Di Falco, M. C. Gather, *Nat. Commun.* **2018**, *9*, 4817.
- [276] J. U. Nockel, A. D. Stone, *Nature* **1997**, *385*, 45.
- [277] S. Shinohara, T. Harayama, T. Fukushima, M. Hentschel, T. Sasaki, E. E. Narimanov, *Phys. Rev. Lett.* **2010**, *104*, 163902.
- [278] D. G. Lidzey, D. D. C. Bradley, M. S. Skolnick, T. Virgili, S. Walker, D. M. Whittaker, *Nature* **1998**, *395*, 53.
- [279] A. Das, P. T. Snee, *ChemPhysChem* **2016**, *17*, 598.
- [280] Y. J. Heo, H. Shibata, T. Okitsu, T. Kawanishi, S. Takeuchi, *Proc. Natl. Acad. Sci. USA* **2011**, *108*, 13399.
- [281] H. Cao, J. Y. Xu, E. W. Seelig, R. P. H. Chang, *Appl. Phys. Lett.* **2000**, *76*, 2997.
- [282] T. Nakamura, S. Sonoda, T. Yamamoto, S. Adachi, *Opt. Lett.* **2015**, *40*, 2661.